ABSTRACT

Title of thesis: VELOCITY TRANSFORMATION
FOR COMPRESSIBLE WALL TURBULENCE
WITH HEAT TRANSFER

Andrew Trettel, Master of Science, 2015

Thesis directed by: Professor Johan Larsson
Department of Mechanical Engineering

A transformation is derived that removes the effects of variable properties from wall-bounded turbulent flows. The transformation derives from the logarithmic velocity profile and the universality of the stress balance. The Van Driest transformation and the viscous sublayer transformation form subsets of this proposed transformation. This transformation is validated against direct numerical simulations of compressible turbulent channel flows.

VELOCITY TRANSFORMATION
FOR COMPRESSIBLE WALL TURBULENCE
WITH HEAT TRANSFER

by

Andrew Trettel

Thesis submitted to the Faculty of the Graduate School of the
University of Maryland, College Park in partial fulfillment
of the requirements for the degree of
Master of Science
2015

Advisory Committee:
Professor Johan Larsson, Chair
Professor Ken Kiger
Professor Amir Riaz

Acknowledgements

Contents

List of Tables

List of Figures

Chapter 1

Introduction

What are the correct coordinate and velocity scales for compressible wall-bounded turbulent flows?

In incompressible wall-bounded turbulent flows, the "law of the wall" scaling collapses mean velocity profiles onto roughly the same "universal" profile:

$$\frac{U}{u_\tau} = f\left(\frac{\rho_w u_\tau y}{\mu_w}\right) \tag{1.1}$$

$$U^+ = f(y^+) \tag{1.2}$$

Prandtl and von Kármán originally considered these "plus-unit" scales (see references Prandtl [1925], Kármán [1930], Prandtl [1932], and Prandtl [1933]), but they also emerge from a conventional dimensional analysis of the system (see Langhaar [1951] for more discussion).

These scales are correct for incompressible flows in the inner layer. The inner layer is the region of flow closest to the wall, and the outer layer is the region of the flow farthest from the wall. In the inner layer, the dominant length scale is the viscous length scale $\ell_v = \mu_w/(\rho_w u_\tau)$ due to the presence of the wall; in the outer layer, the dominant length scale is the boundary layer thickness δ due to eddies being roughly that size. In the inner

layer, the "law of the wall" scaling for both coordinate y and velocity U (equation 1.1) works well. The inner layer is special in that it contains the three universal regions of wall-bounded turbulent flow:

$$0 \leq y^+ \leq 5 \qquad \text{Viscous sublayer} \qquad (1.3)$$

$$5 \leq y^+ \leq 40 \text{ to } 50 \qquad \text{Buffer layer} \qquad (1.4)$$

$$50 \leq y^+ \qquad \text{Logarithmic region} \qquad (1.5)$$

Previous research has sought to extend the "law of the wall" scaling to compressible flows by posing another question: What procedure converts compressible flows into equivalent incompressible flows? The goal is to derive a transformation that collapses the entire compressible mean velocity profile onto an equivalent incompressible mean velocity profile in the universal "law of the wall" scaling for all Mach numbers and heat transfer scenarios.

These transformations consider how compressibility alters the flow. Compressibility introduces property variation and compressible effects including acoustics and shock waves. For non-hypersonic flows, the property variation alters the flow more than shocks or acoustics do, so most transformations ignore the compressible effects and concentrate on the property variation (for more discussion of compressible effects, see the reviews of Bradshaw [1977] and Lele [1994]).

Density variation motivates the most successful compressibility transformation, the Van Driest transformation:

$$U_{\text{VD}}^+ = \int_0^{u^+} \left(\frac{\bar{\rho}}{\rho_w} \right)^{1/2} du^+ \qquad (1.6)$$

This equation was developed informally by Van Driest [1951], generalized by Danberg [1964], and popularized by Bradshaw [1977] and Bushnell et al. [1977] and Fernholz et al. [1981]. It accounts for changes in density by transforming the compressible mean velocities back to an incompressible (constant density) state with the same wall normal coordinate y^+. The Van Driest transformation derives from the same arguments as the logarithmic velocity
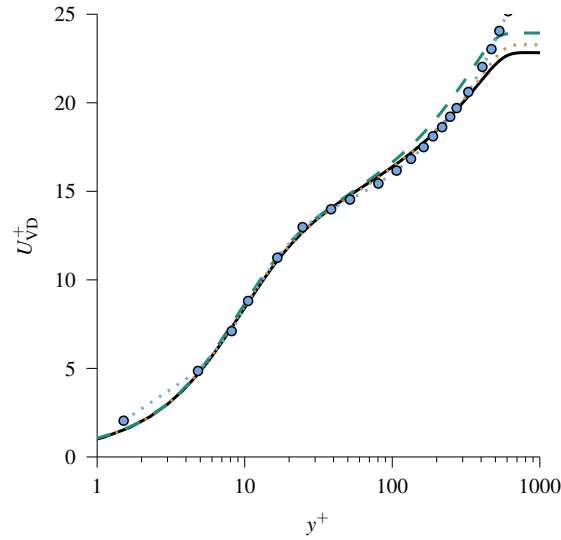
Figure 1.1: The Van Driest transformation applied to adiabatic wall flows, $B_q = 0$.

————, incompressible boundary layer reference at $Re_\tau = 578$ from DNS by Jiménez et al. [2010].

············, Van Driest transformed Mach 2 boundary layer at $Re_\tau = 583$ from DNS by Pirozzoli and Bernardini [2013].

------, Van Driest transformed Mach 4 boundary layer at $Re_\tau = 505$ from DNS by Pirozzoli and Bernardini [2013].

Circles, Van Driest transformed Mach 4.8 boundary layer at $Re_\tau = 1549$ from experiment by Voisinet and Lee [1972] (72020205).

profile:

$$U^+ = \frac{1}{\kappa} \log y^+ + C \tag{1.7}$$

For adiabatic walls — walls through which no heat flows — the Van Driest transformation collapses mean velocity profiles onto the incompressible profiles, as illustrated in figure 1.1. This figure plots both experimental data from Voisinet and Lee [1972] and direct numerical simulation (DNS) data from Pirozzoli and Bernardini [2013] and compares these profiles to an incompressible reference profile from Jiménez et al. [2010]. All 4 curves meld together into the same "law of the wall" profile. This collapse for adiabatic walls is supported by the DNS studies of Guarini et al. [2000], Maeder [2000], Pirozzoli

et al. [2004], Martín [2007], Duan et al. [2011], Lagha et al. [2011], and Pirozzoli and Bernardini [2013].

Another way to examine how well the Van Driest transformation collapses compressible profiles is to look at the log-law intercept C from equation 1.7. For incompressible flows, values of C between 5.2 and 5.5 are normal. After examining most available experimental compressible turbulent boundary layer data, Danberg [1964] concluded (in figure 38) that for adiabatic situations the Van Driest transformed intercept C is independent of the Mach number and matches the incompressible value.

In short, the Van Driest transformation's success for adiabatic wall data has established it as the "accepted standard" for the mean velocity scaling of compressible wall turbulence (Spina et al. [1994]). As an accepted standard, it fits into the current paradigm of transformation concepts for compressible wall turbulence. This current paradigm consists of several components:

Characteristic Reynolds number Re_{δ_2} This Reynolds number $\mathrm{Re}_{\delta_2} = \rho_e u_e \delta_2 / \mu_w$ was derived by Walz [1956] and described in detail in Fernholz and Finley [1980] as the characteristic Reynolds number for comparing two different flow scenarios (for example, for comparing an incompressible flow to a compressible one).

Velocity transformation U_{VD}^{+} with coordinate y^{+} The Van Driest transformation and the untransformed "law of the wall" coordinate $y^{+} = y\rho_w \sqrt{\tau_w/\rho_w}/\mu_w$, as discussed earlier.

Reynolds stress transformation $\bar{\rho} r / \tau_w$ with coordinate y^{*} These scales are Morkovin's scaling and the "semi-local" coordinate scaling $y^{*} = y\bar{\rho}\sqrt{\tau_w/\bar{\rho}}/\bar{\mu}$. Morkovin [1962] originally derived this Reynolds stress scaling (with r being a Reynolds stress component). Huang et al. [1995] observed that Reynolds stresses transformed according to Morkovin's scaling collapse well onto incompressible Reynolds stresses when plotted in the "semi-local" coordinate y^{*}.

These components form the analytical backbone to transform compressible data onto incompressible data. However, they were created over a large span of time — Van Driest [1951] in 1951 to Huang et al. [1995] in 1995 — and despite their success individually, they are unrelated and were created on a somewhat piece-meal basis. For that reason, they clash with each other.

For example, the current paradigm considers two wall-normal coordinates — y^+ for velocities and y^* for fluctuations — and the reason why two different coordinates seem to work has not yet been established. Furthermore, the characteristic Reynolds number Re_{δ_2} works well to compare and contrast different flows, but it remains disconnected from the analyses concerning the velocity transformation and Reynolds stress transformations.

Regardless, the current paradigm as described here works well to transform adiabatic wall-bounded turbulence.

1.1 The failures of the Van Driest transformation

At least one component of this current paradigm breaks down noticeably under reasonable circumstances. The Van Driest transformation does not collapse compressible mean velocity profiles onto incompressible ones when the wall is cooled – that is, when heat leaves the domain through the wall.

In wall-bounded turbulence, a dimensionless measure of wall heat transfer is

$$B_q = \frac{q_w}{\rho_w c_p u_\tau T_w} \tag{1.8}$$

Figure 1.2 plots the incompressible channel DNS of Moser et al. [1999] against two cases of direct numerical simulations run for this present study. The details of the present study are discussed later in chapter 2. Unlike adiabatic boundary layers, the entire profiles no longer match: the lightly cooled $B_q = -0.053$ case stays near the incompressible reference, but the highly cooled $B_q = -0.131$ case veers far from the reference profile.

5
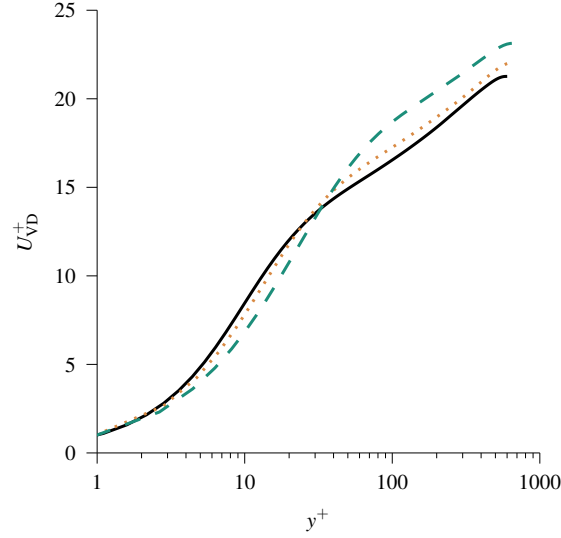
Figure 1.2: The Van Driest transformation applied to cooled wall flows, $B_q < 0$.

————, incompressible channel reference at $\mathrm{Re}_\tau = 587$ from DNS by Moser et al. [1999].

············, Van Driest transformed Mach 1.7 channel at $B_q = -0.053$ and $\mathrm{Re}_\tau = 663$ from present DNS.

------, Van Driest transformed Mach 3.0 channel at $B_q = -0.131$ and $\mathrm{Re}_\tau = 650$ from present DNS.

Increased cooling (increasingly negative B_q reveals two distinct changes in the mean velocity profile:

An upwards shift The log-layer increases in velocity (the intercept C increases). For this thesis, C is defined as

$$C = \frac{1}{y_2^+ - y_1^+} \int_{y_1^+}^{y_2^+} \left(U^+ - \tfrac{1}{\kappa} \log y^+ \right) dy^+ \tag{1.9}$$

An outwards shift The viscous sublayer's slope drops (its slope S decreases). For this thesis, S is defined as

$$S = \frac{1}{4} \int_{y^+=0}^{y^+=4} \frac{dU^+}{dy^+} dy^+ \tag{1.10}$$

6
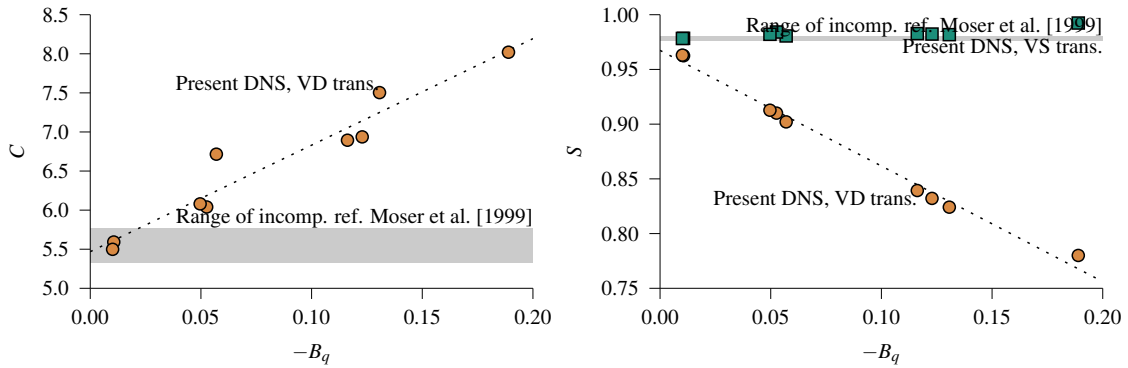
(a) The Van Driest transformed log-law intercept C increases with cooling.

(b) S decreases with cooling

Figure 1.3: Properties of Van Driest transformed mean velocity profiles are functions of wall cooling rate B_q.

Previous researchers noticed the upwards shift in the 1960s. Danberg [1964] noticed the near perfect collapse of adiabatic boundary layers using the Van Driest transformation, but remarked on page 67 that "C increases quite rapidly with heat transfer into the wall," and illustrates this trend in figure 39 of Danberg [1964]. To some degree, the results of Danberg [1964] are exaggerated due to the shear stress at the wall being calculated from the gradient outside the viscous sublayer — it is difficult to place instruments close enough to the wall to measure velocities in the viscous sublayer — but the trend is clear and supported by DNS of cooled wall turbulent flows. The boundary layer DNS of Maeder [2000], the channel DNS of Coleman et al. [1995], and the channel DNS Foysi et al. [2004] all display an increased C in the transformed profiles, but the boundary layer DNS of Duan et al. [2010] shares the same intercept C as the incompressible log-law.

Figure 1.3a depicts a scatter-plot with cooling rate $-B_q$ on the horizontal axis and the Van Driest transformed log-law intercept C on the vertical axis using data from the present DNS. The shaded region represents the range of C in the incompressible channel reference of Moser et al. [1999]. The data scatter slightly due to a low Reynolds number effect (discussed in chapter 5) but generally increase with cooling.

The outwards shift took longer to notice. In incompressible flow, the viscous sublayer

obeys the profile

$$U^+ = y^+ \tag{1.11}$$

up to around $y^+ \approx 5$. For cooled flows, however, the viscous sublayer's slope plummets. This drop is evidenced by the most cooled DNS of Duan et al. [2010] and the most cooled boundary layer experiment of Voisinet and Lee [1972] (see figure 8).

Figure 1.3b depicts a scatter-plot with cooling rate $-B_q$ on the horizontal axis and the transformed viscous sublayer slope S on the vertical axis for two different transformations: the Van Driest transformation (equation 1.6) as circles, and the viscous sublayer transformation (equation 1.12) as diamonds. The viscous sublayer transformation derives from a stress balance at the wall, and serves as the parallel to the Van Driest transformation for viscous sublayer. The viscous sublayer transformation is

$$U_{\text{VS}}^+ = \int_0^{u^+} \left(\frac{\bar{\mu}}{\mu_w} \right) du^+ \tag{1.12}$$

The Van Driest transformed S plummets cleanly with cooling, but the viscous sublayer transformed velocity gradient hovers around incompressible reference's (Moser et al. [1999]) range. Ideally, the velocity gradient in the viscous sublayer is 1, matching the viscous sublayer profile (equation 1.11), but this profile is only a fourth-order approximation of the near-wall velocity profile (see Monin and Yaglom [1971] for more information) so the incompressible reference is always slightly below 1 but not far off. Regardless, the viscous sublayer transformation is only correct for the viscous sublayer — it gets the correct S but not C — so the hard part is finding out what works for the entire inner layer.

In addition to these two easily measured shifts, other changes occur when the boundary layer is cooled. The buffer layer tends to grow in size, and the friction Reynolds number Re_τ also tends to grows in size.

1.2 Objectives of the present work

As detailed in the previous section, the Van Driest transformation — the cornerstone of the current paradigm of compressible wall turbulence — behaves incorrectly when the wall is cooled.

If the Van Driest transformation is incorrect, what is the correct transformation to transform compressible mean velocities into equivalent incompressible mean velocities? Recent research by Brun et al. [2008], Zhang et al. [2012], and Pei et al. [2013] looked for an improved transformation that restores universality in wall-bounded compressible turbulent flows, but none of these new works seemed definitive. As discussed previously, many different changes occur with cooling — C increases, S decreases, Re_τ increases — and these changes all suggest that both the transformed velocity U_{VD}^+ and the coordinate y^+ are no longer correct. Therefore, the objective of this thesis is to find a new velocity and coordinate transformation that matches equivalent incompressible profiles for a broad range of Mach numbers and heating or cooling rates.

Developing a new transformations alters the current paradigm, and offers an opportunity to re-examine other problems in the current paradigm, including which Reynolds number characterizes the flow, and what is the proper Reynolds shear stress scaling.

Chapter 2

Numerical setup

To explore new transformation concepts for compressible wall turbulence, 9 different direct numerical simulations (DNS) of compressible turbulent channel flows were run using the DNS code named Hybrid. The Hybrid code is a solution-adaptive central/WENO scheme finite-difference code for 6th/5th order accuracy in space. This code has been used in the past for several other compressible turbulence studies — Larsson and Lele [2009], Bermejo-Moreno et al. [2013], and Larsson et al. [2013], for example —- and is described in greater detail in these references.

This research was conducted on Deepthought2, a high-performance computing cluster maintained by the University of Maryland Department of IT.

2.1   Physical setup of channels

Channels are an ideal situation to easily generate wall-cooled DNS data over a large range of cooling rates and Reynolds numbers. Two properties of compressible channel flows make them ideal for a DNS study of wall cooling on turbulence:

1. Channels reach fully-developed turbulence easily by using periodic boundary conditions and letting the outflow serve as the inflow. Eventually, without much trial and

error, the channel transitions and reaches a statistically stationary state in the channel that is easy to average over.

2. Channels offer an easy way to control the cooling rate in a compressible wall-bounded flow, since the Mach number directly determines the cooling rate. Viscous dissipation is controlled by the Mach number and heats the flow, reaching a temperature of T_c at the center of the channel. This heat leaves the domain through the isothermal channel walls. The wall temperature T_w is constant and arbitrary, since the centerline temperature T_c will always be higher due to viscous heating, so only the ratio T_c/T_w matters ultimately. In short, the higher the Mach number, the more cooled the channel is.

The wall heat transfer parameter B_q (equation 1.8) can be rewritten as

$$B_q = -\frac{1}{\text{Pr}} \frac{d(\bar{T}/T_w)}{dy^+}\bigg|_w \tag{2.1}$$

so it is clear that B_q describes the wall heat transfer well, since for higher T_c/T_w, the temperature gradient (and therefore the magnitude of B_q) increases.

2.2   Reach and span of DNS study

The present DNS study considered 3 sets of transformed Reynolds numbers (the transformed Reynolds number Re_τ^* is defined in equation 5.1). Each transformed Reynolds number has 3 cases, from low to high cooling rate. The transformed Reynolds numbers Re_τ^* were chosen to match the incompressible turbulent channel DNS data of Moser et al. [1999]. Therefore, the DNS data of Moser et al. [1999] serves as a direct incompressible comparison to the present compressible cases.

In all cases, $\text{Pr} = 0.7$, $\gamma = 1.4$, and the domain size was $[\ell_x, \ell_y, \ell_z]/h = [10, 2, 3]$.

Table 2.1 lists all 9 DNS cases in the present channel DNS. These cover a range of

Table 2.1: Quantities from present channel DNS

Casename	Ma	Re_h	Re_τ	Re_τ^*	$-B_q$	T_c/T_w	n_x	n_y	n_z	Δx^+	Δy_{min}^+	$\Delta y_{max}/h$	Δz^+
M0.7R400	0.7	7500	437.4	396.4	0.011	1.082	416	176	208	10.515	0.855	0.0180	6.309
M0.7R600	0.7	11750	652.1	591.1	0.010	1.082	608	256	320	10.725	0.875	0.0124	6.113
M1.7R200	1.7	4500	321.6	196.6	0.057	1.483	304	128	160	10.579	0.867	0.0247	6.030
M1.7R400	1.7	10000	663.1	406.3	0.053	1.481	800	246	400	8.288	0.926	0.0129	4.973
M1.7R600	1.7	15500	971.7	595.8	0.050	1.480	896	384	480	10.845	0.868	0.0082	6.073
M3.0R200	3.0	7500	649.9	208.3	0.131	2.487	608	256	320	10.689	0.872	0.0124	6.093
M3.0R400	3.0	15000	1232.5	395.5	0.123	2.486	1152	480	576	10.699	0.880	0.0066	6.419
M3.0R600	3.0	24000	1876.1	600.7	0.116	2.491	1728	416	896	10.857	0.849	0.0093	6.282
M4.0R200	4.0	10000	1017.5	202.8	0.189	3.637	1260	384	644	8.075	0.909	0.0082	4.740

Mach numbers from 0.7 to 4.0, and a range of Re_h from 4500 to 24000.

Again, notice the direct relationship between $-B_q$ and T_c/T_w. For these isothermal wall channels, the temperature itself does not matter much to set the cooling rate, but the ratio of temperatures does.

2.3 Grid convergence

The M4.0R200 case served as the basis for the other 8 channels' grid sizes. This case had several properties that required its grid to be the strictest:

It engages the WENO scheme the most. M4.0R200 has the highest Mach number. It will generate the most shocks, and to capture these shocks correctly, the WENO scheme needs to be engaged more as the Mach number increases. WENO schemes are highly dissipative and in the Hybrid code are only 5th-order accurate — in contrast, the central scheme is 6th-order accurate. M4.0R200 therefore requires additional precision over the other cases to resolve all the scales correctly without dissipation altering the results.

Its temperature changes the most. For M4.0R200, $T_c/T_w = 3.637$. The density and viscosity change drastically from the wall to the channel center.

Its transformed friction Reynolds number changes the most. $Re_\tau^* = 203$ compared to $Re_\tau = 1018$, so the coordinate changes the most and requires a stricter grid to properly resolve this extreme change in the coordinates.

12

For these reasons, the `M4.0R200` case requires the strictest grid requirements out of all 9 cases considered, so this case's relevant grid scales (Δx^+, $\Delta y^+_{\min}$, $\Delta y/h$, and Δz^+) need to be the strictest and smallest. All other cases would not require this level of refinement, and as seen in table 2.1 were at similar levels of refinement.

Figure 2.1a shows the grid convergence of the Van Driest transformed velocity profiles for `M4.0R200`, and figure 2.1a shows the grid convergence of the dimensionless $\widetilde{u'v'}$ Reynolds stress. The symbols correspond to the grid sizes in table 2.2. Only grid C disagreed slightly in the Van Driest transformed velocity profile (by much less than 1 in U^+_{VD}), and only far from the wall. All other grids followed each other closely despite the large change in grid resolution, strongly suggesting grid independence.
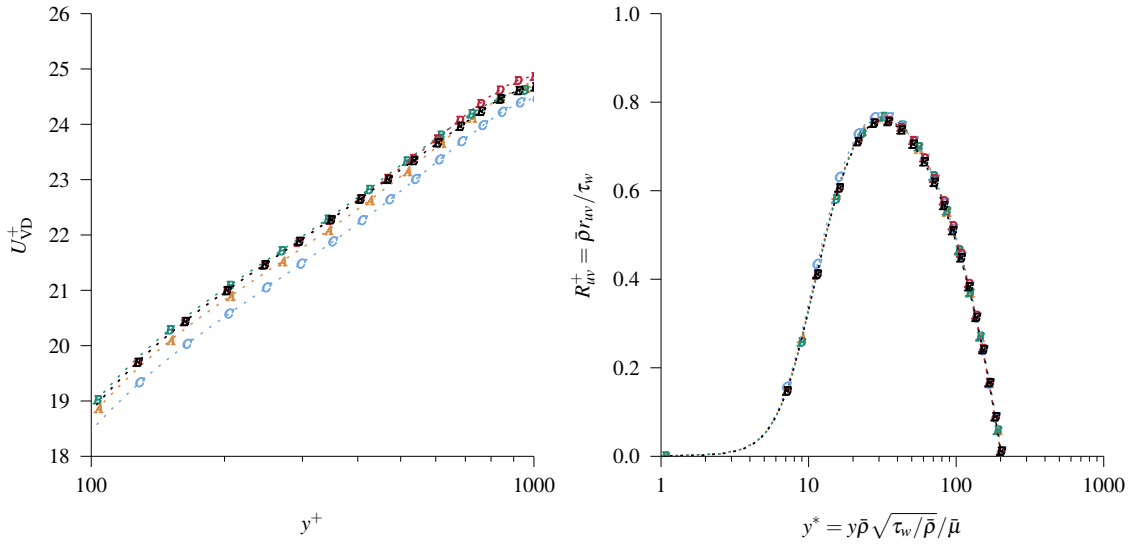
(a) Van Driest transformed velocity profiles, U_{VD}^+. This figure is zoomed in onto the log-law to show the slight difference between grids C and A, B, D, and E.

(b) Reynolds stress profiles, $\bar{\rho}\widetilde{u'v'}/\tau_w$

Figure 2.1: Grid convergence of M4.0R200. The letters correspond to the grid sizes given in table 2.2.

Table 2.2: Grid sizes for M4.0R200

Label	n_x	n_y	n_z	Δx^+	$\Delta y_{\min}^+$	$\Delta y_{\max}/h$	Δz^+
A	620	272	272	16.467	1.289	0.0116	11.261
B	940	272	480	10.799	1.281	0.0116	6.344
C	760	384	380	13.571	0.921	0.0082	8.143
D	940	384	480	10.789	0.906	0.0082	6.339
E	1260	384	644	8.075	0.909	0.0082	4.740

Chapter 3

Derivation of proposed transformation

3.1 Notation

The goal of this thesis is to develop a method to collapse compressible mean velocity profiles onto incompressible ones, so it is important to distinguish between two states:

an incompressible state with constant reference density ρ_w and constant reference viscosity μ_w, and

a compressible state with spatially-varying mean density $\bar{\rho}$ and mean viscosity $\bar{\mu}$.

The incompressible reference state is the wall values of density and viscosity. So the goal is to convert a flow with variable properties into one that has the same properties as the values at the wall.

The rest of the notation is

Capitalized letters and variables with a $*$ superscript are incompressible, transformed, constant property values. For example, velocity U, coordinate Y, Reynolds stress R, and friction Reynolds number Re_τ^*.

Lowercase letters and variables without a $*$ superscript are compressible, untransformed, variable property values. For example, velocity u, coordinate y, Reynolds stress r,

and friction Reynolds number Re_τ.

Plus-units denote dimensionless values, which are dimensional values divided by their corresponding scale. There is only one friction velocity u_τ and one viscous length scale ℓ_ν shared by both the incompressible and compressible states. These are

$$u_\tau = (\tau_w/\rho_w)^{1/2} \tag{3.1}$$

$$\ell_\nu = \mu_w/(\rho_w u_\tau) \tag{3.2}$$

From these two scales, the velocity scale is u_τ, the coordinate scale is ℓ_ν, and the Reynolds stress scale is u_τ^2.

Universal variables are transformed dimensionless values, so they are capitalized with plus-units. The goal is to develop a method to arrive at these universal variables. In this notation, this goal is to go from untransformed, compressible, dimensional values to transformed, incompressible, dimensionless values (universal values):

$$
\begin{aligned}
y &\to Y^+ \\
u &\to U^+
\end{aligned}
\tag{3.3}
$$

All of this notation is compared in table 3.1.

Untransformed, compressible, dimensional	u	y	τ	r	
Untransformed, compressible, dimensionless	u^+	y^+		r^+	Re_τ
Transformed, incompressible, dimensional	U	Y	τ^*	R	
Transformed, compressible, dimensionless and universal	U^+	Y^+		R^+	Re_τ^*

Table 3.1: Notation

3.2 Transformation basics

This goal motivates a search for a coordinate transformation and a velocity transformation, both generalized as differential transformations operating directly on velocity gradients.

16

The chain rule reveals how these transformations change the gradients:

$$\frac{dU}{dY} = \frac{dU}{du}\frac{dy}{dY}\frac{du}{dy} \qquad (3.4)$$

Here, the transformed velocity gradient dU/dY is a function of the velocity transformation dU/du, the coordinate transformation dY/dy, and the untransformed velocity gradient du/dy. To obtain the coordinate and velocity, integrate the transformation functions:

$$U^+ = \int_0^{u^+} \frac{dU}{du}du^+, \qquad\qquad Y^+ = \int_0^{y^+} \frac{dY}{dy}dy^+. \qquad (3.5)$$

Given the definition of the dimensionless units (equations 3.1 and 3.2), the transformation functions in this thesis have the property that

$$\frac{dU}{du} = \frac{dU^+}{du^+}, \qquad\qquad \frac{dY}{dy} = \frac{dY^+}{dy^+}.$$

so for brevity this thesis uses only the dimensional form without plus-units.

Note that all prior transformations can be written in this format. The Van Driest transformation then is $dY/dy = 1$ and $dU/du = (\bar{\rho}/\rho_w)^{1/2}$; the viscous sublayer transformation is $dY/dy = 1$ and $dU/du = (\bar{\mu}/\mu_w)$.

3.3   Derivation of log-law condition

This thesis derives the proposed transformation in three parts. First, a condition from the log-law is derived. Second, a stress balance condition is derived. And lastly, these two conditions combine to obtain the full transformation.

The log-law condition comes first. Van Driest [1951] and Danberg [1964] considered a similar condition (see section B for others), which they used to derive the Van Driest transformation. More recently, Brun et al. [2008] considered a more general form of this

condition that includes the possibility of a coordinate transformation. This section generalizes all of this previous work.

Now, consider the compressible log-law velocity gradient. Previous researchers have derived this gradient using many methods, but the dimensional analysis of Bradshaw [1994] explains the important variables and their relationships well. In the turbulent region of the flow, viscosity $\bar{\mu}$ is unimportant; the important variables are the shear stress at the wall τ_w, the local density $\bar{\rho}$, and the distance from the wall y, as per Townsend's attached eddy hypothesis. Dimensional analysis then obtains a velocity scale $\sqrt{\tau_w/\bar{\rho}}$ and a length scale y. In the form of a velocity gradient, these two variables yield

$$\frac{du}{dy} = \frac{1}{\kappa}\frac{1}{y}\left(\frac{\tau_w}{\bar{\rho}}\right)^{1/2} \tag{3.6}$$

Multiply by Y/Y and $(\rho_w/\rho_w)^{1/2}$:

$$\frac{du}{dy} = \frac{1}{\kappa}\frac{Y}{Y}\frac{1}{y}\left(\frac{\tau_w}{\bar{\rho}}\right)^{1/2}\left(\frac{\rho_w}{\rho_w}\right)^{1/2} \tag{3.7}$$

Rearrange and group terms:

$$\frac{du}{dy} = \frac{Y}{y}\left(\frac{\rho_w}{\bar{\rho}}\right)^{1/2}\frac{1}{\kappa}\frac{1}{Y}\left(\frac{\tau_w}{\rho_w}\right)^{1/2} \tag{3.8}$$

By analogy to equation 3.6, the incompressible log-law velocity gradient is

$$\frac{dU}{dY} = \frac{1}{\kappa}\frac{1}{Y}\left(\frac{\tau_w}{\rho_w}\right)^{1/2} \tag{3.9}$$

and this gradient simplifies the equation to

$$\frac{du}{dy} = \frac{Y}{y}\left(\frac{\rho_w}{\bar{\rho}}\right)^{1/2}\frac{dU}{dY} \tag{3.10}$$

Solve for the incompressible velocity gradient:

$$\frac{dU}{dY} = \frac{y}{Y}\left(\frac{\bar{\rho}}{\rho_w}\right)^{1/2}\frac{du}{dy} \tag{3.11}$$

This gradient equation is important and enters later. First, it is important to reveal the underlying velocity transformation in this equation. Apply the chain rule to both sides of the equation and cancel out terms:

$$\frac{dU}{du}\frac{d\!\!\!/u}{d\!\!\!/Y} = \frac{y}{Y}\left(\frac{\bar{\rho}}{\rho_w}\right)^{1/2}\frac{dY}{dy}\frac{d\!\!\!/u}{d\!\!\!/y} \tag{3.12}$$

Simplify to obtain the velocity transformation as a function of the coordinate transformation:

$$\frac{dU}{du} = \frac{y}{Y}\left(\frac{\bar{\rho}}{\rho_w}\right)^{1/2}\frac{dY}{dy} \tag{3.13}$$

The Van Driest transformation is a subset of this equation when $dY/dy = 1$.

3.4 Derivation of stress balance condition

Earlier, the chain rule (equation 3.4) revealed that all similar differential transformations — including both the Van Driest and viscous sublayer transformations — operate directly on velocity gradients, and only indirectly operate on the velocities themselves (through integration).

This observation motivates an additional condition involving the velocity gradients themselves. The Van Driest transformation works by adjusting the velocity gradient of a variable density flow to the constant density value. It adjusts the gradients without worrying about the underlying physical mechanisms that determine their values. In other words, the Van Driest transformation obtains the correct slope while violating the stress balance (momentum conservation). Any change in the velocity gradient changes the viscous stresses, disrupting the stress balance. This fact motivates seeking to preserve the stress balance

between the untransformed and transformed states.

So, where does a stress balance equation come from? For Newtonian fluids, the compressible Navier-Stokes equations can be simplified and integrated to yield several equations with roughly the same form. These equations provide an approximately correct stress balance condition for the entire inner layer.

For zero pressure gradient boundary layers, analysis of the region close to the wall (see Cebeci and Smith [1974] on pages 113 to 114 and 143 to 144 for more details) obtains.

$$\mu \overline{\frac{du}{dy}} - \overline{\rho u'' v''} \approx \tau_w \tag{3.14}$$

For channels, integration of the momentum equation obtains

$$\mu \overline{\frac{du}{dy}} - \overline{\rho u'' v''} = \tau_w \left(1 - \frac{y}{h}\right) \approx \tau_w \tag{3.15}$$

which is approximately equal to τ_w for $y/h \ll 1$.

Here, variables with double-primes are Reynolds-averaged fluctuations, and variables with single-primes (as seen later) are Favre-averaged (mass-averaged) fluctuations. For more information on this notation, see page 53 of Cebeci and Smith [1974] or page 63 of Smits and Dussauge [2006].

For both channels and boundary layers, the form of the stress balance comes to

$$\mu \overline{\frac{du}{dy}} - \overline{\rho u'' v''} = \tau_{\text{total}} \approx \text{constant} \tag{3.16}$$

How correct is this equation? To characterize its correctness, non-dimensionalize the incompressible version of equation 3.16 to obtain

$$\frac{dU^+}{dY^+} - R_{uv}^+ = \frac{\tau_{\text{total}}}{\tau_w} \approx 1 \tag{3.17}$$

(a) Low Re_τ, Jiménez et al. [2010]

(b) High Re_τ, Sillero et al. [2013]
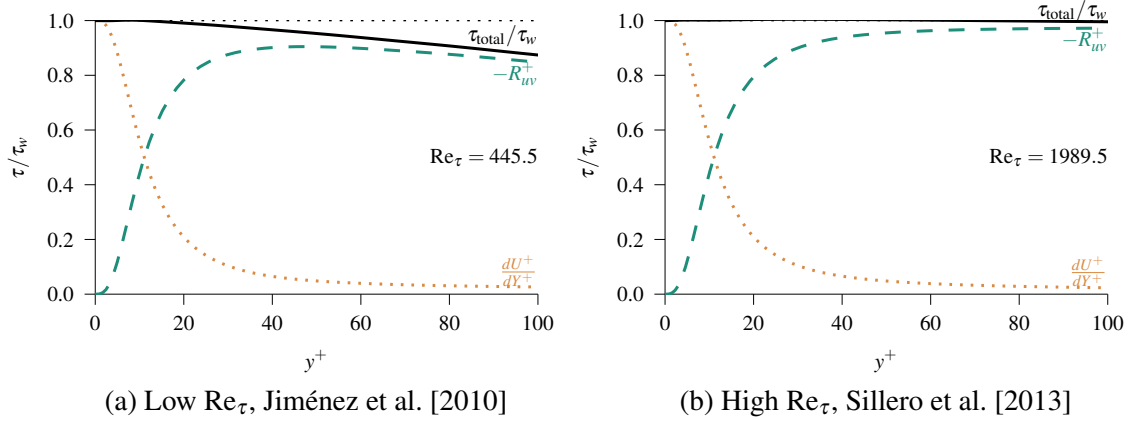
Figure 3.1: Near-wall stress balance for incompressible boundary layers

(a) Low Re_τ, Moser et al. [1999]

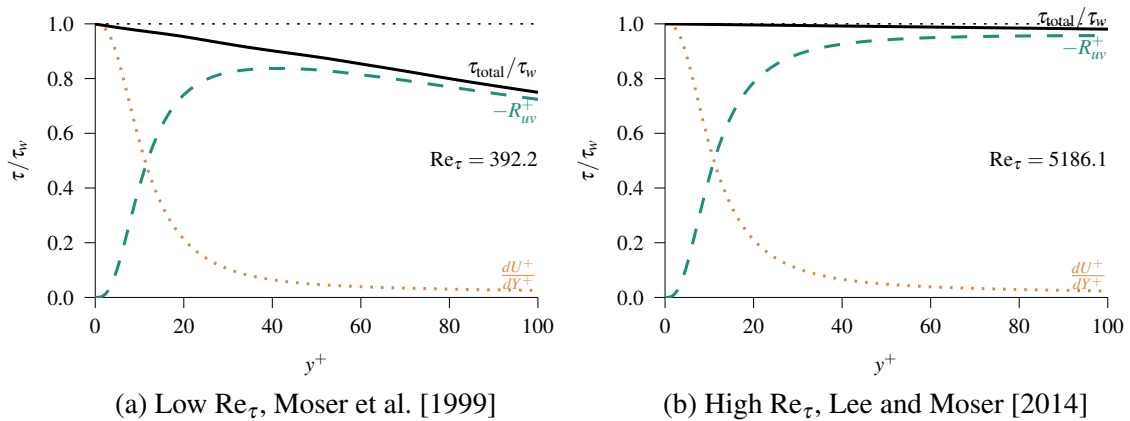(b) High Re_τ, Lee and Moser [2014]

Figure 3.2: Near-wall stress balance for incompressible channels

Now, compare this dimensionless stress balance (equation 3.17) to figures 3.1 and 3.2. Figure 3.1 checks the validity of this equation for low and high Reynolds number boundary layers, and figure 3.2 checks the validity of this equation for low and high Reynolds number channels. For low Reynolds number flows, this equation remains mostly valid until around $y^+ \approx 50$; for high Reynolds number flows, this equation should be valid throughout the entire inner layer, since the curve for $\tau_{\text{total}}/\tau_w$ barely deviates from 1. So in general, this simple stress balance is valid for the inner layer.

Now, the stress balance given in equation 3.16 is in an difficult to use form, so simplification is the next step. Favre-averaging simplifies the second term:

$$\overline{\rho u'' v''} = \bar{\rho} \widetilde{u' v'} \tag{3.18}$$

The first term simplifies for low turbulent Mach numbers (see Smits and Dussauge [2006] pages 73 to 75 for reference):

$$\overline{\mu \frac{du}{dy}} = \bar{\mu} \frac{d\tilde{u}}{dy} \tag{3.19}$$

Here, the mean velocity is Favre-averaged, but the log-law condition (equation 3.6) only considers Reynolds-averaged velocities. Cebeci and Smith [1974] on pages 73 to 74 argue that for a boundary layer approximation — applicable to channels too — mass flux fluctuations in the x-direction are small compared to the overall mean density, so

$$\tilde{u} - \bar{u} = \frac{\overline{\rho'' u'}}{\bar{\rho}} \approx 0 \tag{3.20}$$

so the Favre-averaged velocity $\tilde{u}$ equals the Reynolds-averaged velocity $\bar{u}$ (but only for velocities in the x direction). The final stress balance equation comes to

$$\bar{\mu} \frac{d\bar{u}}{dy} - \bar{\rho} \widetilde{u' v'} = \tau_{\text{total}} \tag{3.21}$$

Now here is the important part of this derivation: set the universal stress balance equal to the compressible stress balance. What this step means is that the total stress balance is assumed to be universal, the same between the untransformed variable-property case and an equivalent transformed constant property case.

$$\tau^*_{\text{total}} = \tau_{\text{total}} \tag{3.22}$$

$$\mu_w \frac{dU}{dY} - \rho_w R_{uv} = \bar{\mu} \frac{du}{dy} - \bar{\rho} r_{uv} \tag{3.23}$$

This equation is quite powerful. In fact, it can derive two seemingly disconnected ideas: Morkovin's scaling for the Reynolds stresses, and the viscous sublayer transformation. And it also derives the stress balance condition used in the proposed transformation.

First, before arriving at this final stress balance condition, the Reynolds stresses need to be addressed.

Equation 3.23 acts as a general stress balance and relates both the incompressible and compressible states and the viscous stresses and turbulent stresses. As shown in figures 3.1 and 3.2, the Reynolds stress R^+_{uv} tends towards a constant value near 1 at high Reynolds number. R^+_{uv} always starts at zero, so to develop a reasonably proper scaling for this Reynolds shear stress, only the peak magnitude needs to be accounted for — provided a proper coordinate scaling is used, of course.

Naively, turbulence flattens the velocity profile. Where turbulence dominates — where the Reynolds shear stress R^+_{uv} reaches its peak — the viscous stresses are low and viscosity is unimportant, meaning that the velocity gradient itself is small, tending towards zero in fact. This observation helps derive Morkovin's scaling for the Reynolds stresses (see Morkovin [1962]). Use equation 3.23 and presume that both the incompressible velocity gradient dU/dY is nearly zero and that the compressible velocity gradient du/dy is nearly

zero:

$$\mu_w \frac{dU}{dY} - \rho_w R_{uv} = \bar{\mu} \frac{du}{dy} - \bar{\rho} r_{uv}$$

$$\rho_w R_{uv} = \bar{\rho} r_{uv}$$

Non-dimensionalize this equation by dividing by u_τ^2 and then solve for R_{uv}^+:

$$R_{uv}^+ = \frac{\bar{\rho} r_{uv}}{\tau_w} \tag{3.24}$$

This scaling, first derived by Morkovin [1962], is well-known to properly scale the Reynolds stresses in the turbulent region, so it can simplify the general stress balance condition (equation 3.23) into solely a function of velocities.

However, Morkovin's scaling does have a limitation. The limitation is that it does not appear to properly scale R_{uv}^+ in the viscous sublayer or the buffer layer. The derivation shown here reveals why: Morkovin's scaling is only correct for the most turbulent part of the flow. Still, the scaling does have the correct trend — starting from zero and going to the peak value — and for that reason it remains the most correct scaling found so far.

A quick note before moving back to the final stress balance condition: many previous researchers (including Brun et al. [2008]) have presumed that the velocity transformation and the Reynolds stress scaling are the same. That is, they have presumed that $R = (dU/du)r$. Here, no such assumption is made, and the velocity transformation and the Reynolds stress scaling should be independent of each other to yield the most general solution possible.

Now, back to the final stress balance condition. Morkovin's scaling simplifies the final

stress balance condition (equation 3.26) to an adjustment of the velocity gradients:

$$\mu_w \frac{dU}{dY} - \rho_w \overline{R_{uv}} = \bar{\mu} \frac{du}{dy} - \bar{\rho} \overline{r_{uv}} \tag{3.25}$$

$$\mu_w \frac{dU}{dY} = \bar{\mu} \frac{du}{dy} \tag{3.26}$$

A more useful form is the universal velocity gradient:

$$\frac{dU}{dY} = \frac{\bar{\mu}}{\mu_w} \frac{du}{dy} \tag{3.27}$$

If the coordinate remains untransformed (if $Y = y$), this equation becomes the viscous sublayer transformation. However, here the coordinates are presumed to be different, so the action of this equation is quite different — especially since it presumes that Morkovin's scaling for the fluctuations holds — whereas the viscous sublayer transformation presumes that the Reynolds shear stress is always zero. In short, the action of this equation is to maintain the overall stress balance provided that Morkovin's scaling works for Reynolds shear stress.

Still, it is important to note what equation 3.27 does not imply: it does not imply that viscosity is important in the fully turbulent zone. In fact, the opposite is true. Equation 3.27 adjusts the velocity gradients to obey a transformed stress balance. But in the fully-turbulent zone, as noted in the previous derivation of Morkovin's scaling, the velocity profile is nearly flat and the viscous stresses are nearly zero. So in effect, no adjustment due to viscosity happens here (or no large adjustment, at least) since nearly zero times any order-one quantity is still nearly zero. In short, the viscous stresses approach zero far from the wall and only the smallest possible adjustment due to viscosity will occur in the fully turbulent zone.

3.5 Final steps to derive proposed transformation

Set the log-law velocity gradient condition (equation 3.11) equal to the stress balance velocity gradient condition (equation 3.27):

$$\frac{dU}{dY} = \frac{y}{Y}\left(\frac{\bar{\rho}}{\rho_w}\right)^{1/2}\frac{du}{dy} = \frac{\bar{\mu}}{\mu_w}\frac{du}{dy} \tag{3.28}$$

This obtains

$$\frac{\bar{\mu}}{\mu_w} = \frac{y}{Y}\left(\frac{\bar{\rho}}{\rho_w}\right)^{1/2} \tag{3.29}$$

which directly reveals the transformed and dimensional coordinate Y:

$$Y = \left(\frac{\mu_w}{\bar{\mu}}\right)\left(\frac{\bar{\rho}}{\rho_w}\right)^{1/2}y \tag{3.30}$$

The universal coordinate (transformed and dimensionless) then comes to

$$Y^+ = \frac{\bar{\rho}(\tau_w/\bar{\rho})^{1/2}y}{\bar{\mu}} = \frac{y(\tau_w\bar{\rho})^{1/2}}{\bar{\mu}} \tag{3.31}$$

This coordinate is known as "semi-local" coordinate scaling. Researchers have studied it before — including by Lobb et al. [1955] — but the most important observation about it came from Huang et al. [1995], who called it y^* and showed that it correctly scales the fluctuations. Huang et al. [1995] and its companion paper Coleman et al. [1995] argued that this coordinate only works to scale the fluctuations and that the standard coordinate y^+ and the Van Driest transformed velocity U_{VD}^+ correctly scale the mean velocities.

Here, this thesis derived this coordinate by only considering the mean velocities and Morkovin's scaling, making this coordinate a direct consequence of assuming that the transformed log-law obeys a transformed stress balance. Ultimately, this result suggests that "semi-local" scaling will correctly scale the velocities too, provided the correct transformation is used.

This corresponding velocity transformation emerges from the two conditions. Use the chain rule to solve for dU/du in equations 3.11 or 3.27:

$$\frac{dU}{du} = \frac{y}{Y}\left(\frac{\bar{\rho}}{\rho_w}\right)^{1/2}\frac{dY}{dy} \tag{3.32}$$

$$\frac{dU}{du} = \left(\frac{\bar{\mu}}{\mu_w}\right)\frac{dY}{dy} \tag{3.33}$$

Differentiating equation 3.30 obtains the coordinate transformation:

$$\frac{dY}{dy} = \left(\frac{\mu_w}{\bar{\mu}}\right)\left(\frac{\bar{\rho}}{\rho_w}\right)^{1/2}\left[1 + \frac{1}{2}\frac{1}{\bar{\rho}}\frac{d\bar{\rho}}{dy}y - \frac{1}{\bar{\mu}}\frac{d\bar{\mu}}{dy}y\right] \tag{3.34}$$

Plug the transformed coordinate (equation 3.31) and the coordinate transformation (equation 3.34) into the log-law velocity transformation equation (equation 3.13) to obtain

$$\frac{dU}{du} = \left(\frac{\bar{\rho}}{\rho_w}\right)^{1/2}\left[1 + \frac{1}{2}\frac{1}{\bar{\rho}}\frac{d\bar{\rho}}{dy}y - \frac{1}{\bar{\mu}}\frac{d\bar{\mu}}{dy}y\right] \tag{3.35}$$

This equation contains several property gradients that are difficult to measure experimentally. Section 4 details an alternative form of this equation that is mathematically identical but does not require property gradients.

So, in summary, the complete transformation in closed-form is

$$Y^+ = \frac{\bar{\rho}(\tau_w/\bar{\rho})^{1/2}y}{\bar{\mu}}$$

$$U^+ = \int_0^{u^+}\left(\frac{\bar{\rho}}{\rho_w}\right)^{1/2}\left[1 + \frac{1}{2}\frac{1}{\bar{\rho}}\frac{d\bar{\rho}}{dy}y - \frac{1}{\bar{\mu}}\frac{d\bar{\mu}}{dy}y\right]du^+$$

$$R_{uv}^+ = \frac{\bar{\rho}r_{uv}}{\tau_w}$$

$$\mathrm{Re}_\tau^* = \underbrace{\frac{\rho_c(\tau_w/\rho_c)^{1/2}h}{\mu_c}}_{\text{For channels}} = \underbrace{\frac{\rho_e(\tau_w/\rho_e)^{1/2}\delta}{\mu_e}}_{\text{For boundary layers}}$$

Chapter 4

Implementation of proposed transformation

Equation 3.35 is the proposed velocity transformation in closed-form, but it remains difficult to use on computational or experimental data sets. Instead, it can be re-written in a second, equivalent way. The stress balance condition (equation 3.26) is

$$\mu_w \frac{dU}{dY} = \bar{\mu} \frac{du}{dy} \tag{4.1}$$

Apply the chain rule on the left and right hand sides of the equation:

$$\mu_w \frac{dU}{du} \frac{du}{dY} = \bar{\mu} \frac{dY}{dy} \frac{du}{dY} \tag{4.2}$$

$$\frac{dU}{du} = \frac{\bar{\mu}}{\mu_w} \frac{dY}{dy} \tag{4.3}$$

Equation 4.4 is mathematically identical to 3.35 (the "long" method), but in an unclosed form. To use the transformation, the coordinate $Y^+ = y^*$ must be calculated, so calculating its gradient requires little extra work.

$$U^+ = \int_0^{u^+} \left(\frac{\bar{\mu}}{\mu_w} \right) \frac{dY}{dy} du^+ = \int_0^{u^+} \left(\frac{\bar{\mu}}{\mu_w} \right) \frac{dY^+}{dy^+} du^+ \tag{4.4}$$

28
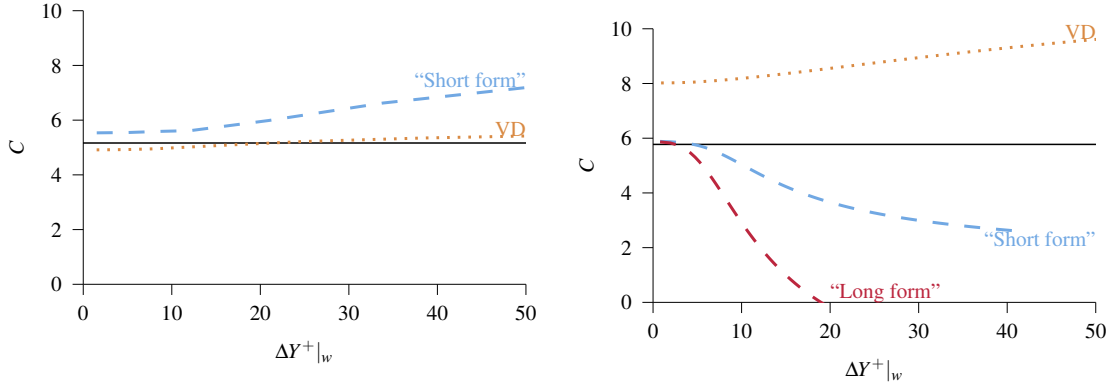
(a) Adiabatic experiment, `72020205` (Voisinet and Lee [1972])

(b) Cooled DNS, `M4.0R200`

Figure 4.1: Intercept robustness for increasingly incomplete data sets

To transform data using this "short" method, use these three steps:

1. Calculate the transformed coordinate $Y^+ = y^* = y\bar{\rho}\sqrt{\tau_w/\bar{\rho}}/\bar{\mu}$ (equation 3.31).

2. Calculate $dY/dy = dY^+/dy^+$ numerically.

3. Calculate the transformed velocity (equation 4.4).

It is also possible to calculate steps 2 and 3 together when using a simple quadrature method as well.

This "short" form of the transformation is more robust than the "long" form on incomplete data sets. A data set is incomplete if it is missing points in the viscous sublayer or buffer layer.

Figures 4.1a and 4.1b compare the robustness of the Van Driest transformation, the "long" form of the proposed transformation, and the "short" form of the proposed transformation as data is removed from the viscous sublayer up through the buffer layer. These plots compare the transformed value of the log-law intercept C against ΔY^+, the location of the first non-wall point in the flow.

For the adiabatic experimental data in figure 4.1a, both the Van Driest transformation and the "short" form of the proposed transformation agree well with the incompressible

29

reference (black line) until around $\Delta Y^+ \approx 10$, at which point the "short" form of the proposed transformation becomes less accurate. The Van Driest transformed value of C does not change appreciably over the interval, indicating that the Van Driest transformation is robust even when the viscous sublayer and buffer layer are missing from the data.

This same pattern occurs in the cooled-wall DNS data in figure 4.1b. Here, the Van Driest transformation fails to match the correct transformed value of C. Both the "short" form and the "long" form of the proposed transformation do match the incompressible reference value of C, but the "long" form's value of C plummets after $\Delta Y^+ \approx 5$, while the "short" form's value of C drops after $\Delta Y^+ \approx 10$. The Van Driest transformed value of C is inaccurate, but it does not change as much as the proposed transformation does over the interval, indicating again that the Van Driest transformation is robust.

In both figures, however, the proposed transformation is the only transformation that works in both adiabatic and cooled scenarios. Its values of C in both are very close to the incompressible reference when the data set is mostly complete.

What conclusions should you draw from these two figures? The main conclusion is that even if τ_w or c_f is measured correctly, as it is in these cases, the proposed transformation will not transform the data correctly if there are no points below $Y^+ \approx 10$. The proposed transformation does not work for incomplete data sets, while the Van Driest transformation works well for incomplete data sets, provided of course that the data is for adiabatic wall boundary layers.

In practical terms, this conclusion means that the proposed transformation will incorrectly transform some experimental data, despite being much more accurate, since many experimental data sets exclude the viscous sublayer and start around $y^+ = 20$. For this reason, this thesis has chosen experimental data to validate against that tends to have points in the viscous sublayer, and this requirement limits the experimental data that can be used to validate the transformation.

Chapter 5

Discussion of proposed transformation

To validate the proposed transformation, its performance is compared against the Van Driest transformation using data from the present DNS study and data from experiments available in Fernholz and Finley [1977] and Fernholz et al. [1981].

After validation, several properties of the transformation will be discussed.

5.1   Numerical validation

Details for all 9 DNS cases are in table 5.1. First, consider the performance of the proposed transformation for 3 specific cases: Mach 4 and $\mathrm{Re}_h = 10000$, Mach 3 and $\mathrm{Re}_h = 15000$, and Mach 3 and $\mathrm{Re}_h = 24000$. These are the 3 most cooled cases for each transformed friction Reynolds number Re_τ^*.

The plots include 3 quantities: the mean velocity profiles, to show the highly improved collapse using the proposed transformation; the velocity gradients, to show the viscous stress aspect of the stress balance; and the dimensionless transformed Reynolds stress R_{uv}^+, to show the turbulent stress aspect of the stress balance. These plots are figures 5.1 to 5.3.

In all three cases, the proposed transformation collapses the mean velocity profiles excellently, as previously discussed by the excellent agreement of transformed C and S. The velocity gradient plots are important for two reasons: the gradients form an important

31
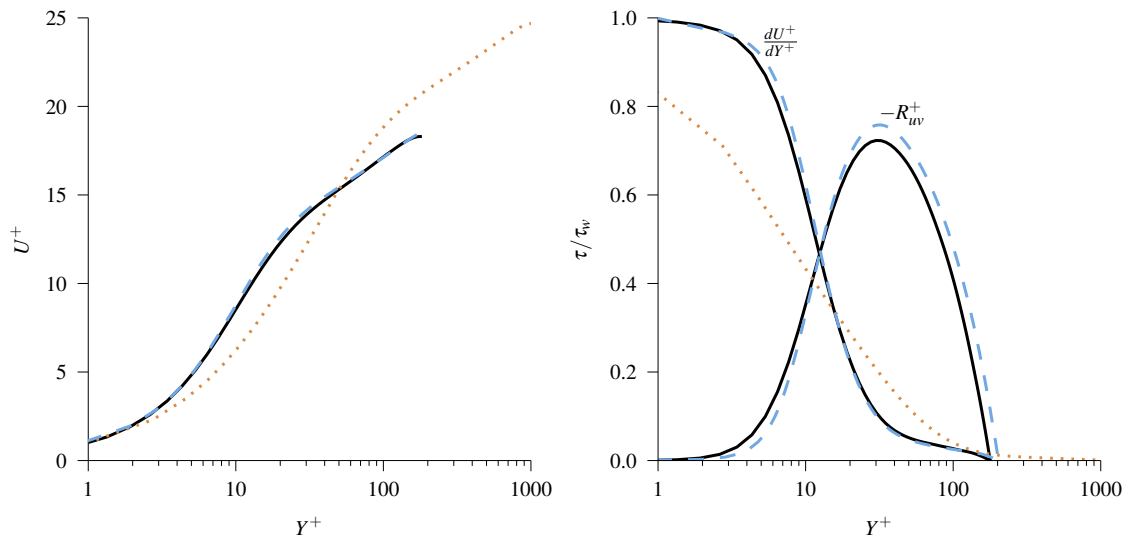
(a) Transformed mean velocities

(b) Transformed stress balance components

Figure 5.1: Velocity, velocity gradient, and Reynolds stress profiles of the $Ma = 4.0$ and $Re_h = 10000$ case.

———, incompressible reference Moser et al. [1999] ($Re_\tau = 178$).

············, present DNS data transformed with Van Driest transformation ($Re_\tau = 1017$).

- - - - -, present DNS data transformed with proposed transformation ($Re_\tau^* = 203$).
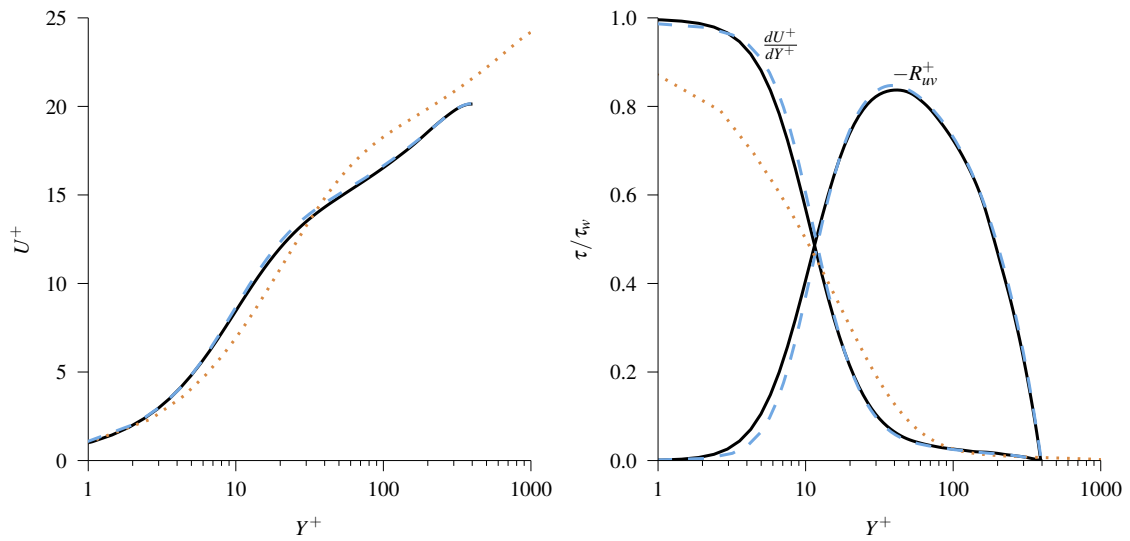
(a) Transformed mean velocities (b) Transformed stress balance components

Figure 5.2: Velocity, velocity gradient, and Reynolds stress profiles of the $Ma = 3.0$ and $Re_h = 15000$ case.

———, incompressible reference Moser et al. [1999] ($Re_\tau = 392$).

··········, present DNS data transformed with Van Driest transformation ($Re_\tau = 1232$).

‑ ‑ ‑ ‑ ‑, present DNS data transformed with proposed transformation ($Re_\tau^* = 396$).
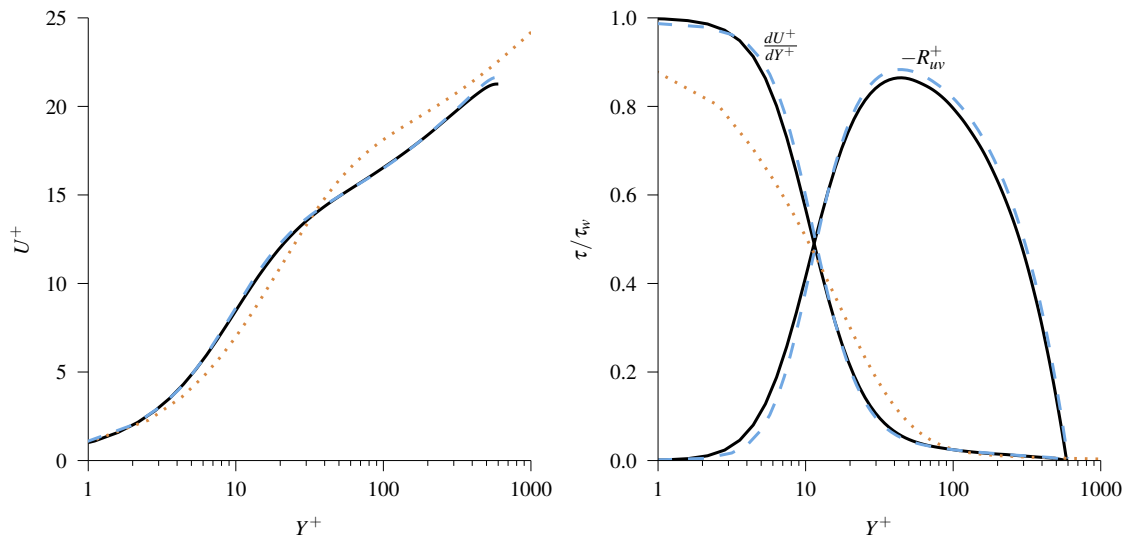
(a) Transformed mean velocities (b) Transformed stress balance components

Figure 5.3: Velocity, velocity gradient, and Reynolds stress profiles of the $\text{Ma} = 3.0$ and $\text{Re}_h = 24000$ case.

————, incompressible reference Moser et al. [1999] ($\text{Re}_\tau = 587$).

············, present DNS data transformed with Van Driest transformation ($\text{Re}_\tau = 1876$).

— — — — , present DNS data transformed with proposed transformation ($\text{Re}_\tau^* = 601$).

Table 5.1: Results of present compressible DNS

Casename	Ma	Re_h	Re_τ	Re_τ^*	$-B_q$	C_{VD}	C_{proposed}	S_{VD}	S_{VS}	S_{proposed}
M0.7R400	0.7	7500	437.4	396.4	0.011	5.592	5.472	0.963	0.978	0.978
M0.7R600	0.7	11750	652.1	591.1	0.010	5.499	5.384	0.963	0.978	0.978
M1.7R200	1.7	4500	321.6	196.6	0.057	6.716	6.017	0.902	0.981	0.977
M1.7R400	1.7	10000	663.1	406.3	0.053	6.040	5.427	0.910	0.984	0.982
M1.7R600	1.7	15500	971.7	595.8	0.050	6.080	5.461	0.913	0.982	0.978
M3.0R200	3.0	7500	649.9	208.3	0.131	7.503	5.913	0.824	0.982	0.976
M3.0R400	3.0	15000	1232.5	395.5	0.123	6.937	5.429	0.832	0.982	0.976
M3.0R600	3.0	24000	1876.1	600.7	0.116	6.894	5.406	0.839	0.983	0.977
M4.0R200	4.0	10000	1017.5	202.8	0.189	8.020	5.883	0.780	0.992	0.984

part of the stress balance, and more importantly, they show where transformations fail locally. The mean velocity profiles lack this property, because errors are cumulative. In all 3 velocity gradient plots, the largest errors in the Van Driest transformed velocity gradient are in the viscous sublayer and buffer layer, but the gradient in the log-law is correct because the Van Driest transformation derives directly from the log-law velocity gradient. The fact that the Van Driest transformation strongly disagrees with the velocity gradients in highly cooled cases motivates a stress balance condition, since it becomes clear that the Van Driest transformation changes the gradients and then therefore the viscous stresses themselves.

The proposed transformation, even at high cooling, agrees throughout both the velocity profiles and the velocity gradients, due to the fact that it considers the stress balance in the entire inner region rather than just in a single region or ignoring it completely (like the Van Driest transformation).

The Reynolds stress figures agree well. Again, the transformation properly accounts for the Reynolds number effects. The plots disagree minutely, but this disagreement is likely due to the slight mismatch in the reference data's friction Reynolds number Re_τ and the transformed data's transformed friction Reynolds number Re_τ^*. As discussed in the section deriving the stress balance condition (chapter 3.4), Morkovin's scaling for the fluctuations is used here, and it tends to under-predict the Reynolds shear stress in the viscous sublayer and early on in the buffer layer. This under-prediction accompanies an over-prediction in the velocity gradient, but neither discrepancy is enough to prevent the velocity profile from collapsing.

Table 5.2: Results of incompressible DNS of Moser et al. [1999]

Re_τ	C	S
178.1	5.774	0.976
392.2	5.331	0.978
587.2	5.399	0.980

Catalog number	Ma_e	$-B_q$	Re_τ	Re_τ^*	Re_{δ_2}	Re_θ	$c_f \cdot 10^4$	S_{VD}	$S_{proposed}$	Source
65050801	2.200	0.000	2134.5	4899.2	5851.7	9829.2	17.100	-	-	Jackson et al. [1965]
72020205	4.823	0.005	1549.4	13925.1	6962.5	28764.0	7.392	1.039	1.026	Voisinet and Lee [1972]
72021501	4.929	0.069	9675.8	13379.6	21288.0	25494.0	10.800	0.687	0.895	Voisinet and Lee [1972]
73020505	1.400	0.000	41544.4	61500.2	96076.0	122450.0	14.800	-	-	Winter and Gaudet [1973]
7702S0301	3.028	0.042	992.1	1811.8	2479.1	3656.4	23.300	-	-	Laderman and Demetriades [1977]

Table 5.3: Experimental cases considered

So far, the discussion has centered on the three most cooled cases. How does the proposed transformation work on the present DNS data globally, for all cases?

The DNS results for the Van Driest transformation, viscous sublayer transformation, and the proposed transformation are in table 5.1. The table compares the Van Driest transformed values of the log-law intercept C and the viscous sublayer slope S with the results of the proposed transformation. As show in figures 1.3a and 1.3b, the Van Driest transformed log-law intercept C increases with cooling, and the Van Driest transformed velocity gradient in the viscous sublayer S decreases.

The proposed transformation performs remarkably better than the Van Driest transformation when comparing the transformed values of C and S. The Van Driest transformed values of S drop considerably with strong cooling compared to the incompressible reference, but the proposed transformation's values of S remain close to the incompressible reference in all 9 cases. In fact, the proposed transformation always agrees in the viscous sublayer and never suffers from an outwards coordinate shift.

The values of C for the proposed transformation more or less match the corresponding values for a given Re_τ^* in the Moser et al. [1999] data given in table 5.2. These Reynolds number effects are discussed more in section 5.3.

5.2 Experimental validation

Fernholz and Finley [1977] and Fernholz et al. [1981] compiled many sets of experimental boundary layer data, and several of these data sets are used to validate the proposed transformation (see table 5.3). The experimental validation is divided into an adiabatic portion (figure 5.4) and a cooled portion (figure 5.5).

The skin friction values for `65050801`, `73020505`, and `7702S0301` came from their respective compilations as given. The skin friction value for `72020205` was calculated from the gradient at the second point in the data set, which gave the best fit. Given the high resolution of the data in the viscous sublayer, this approximation is reasonable. The skin friction value for `72021501` was the corrected value given in Voisinet [1977] by way of Fernholz and Finley [1980].

Probe effects distort the velocities in the viscous sublayer in `65050801` and `7702S0301`. However, the log-law values are intact and reasonable.

In general in these experimental cases, the proposed transformation works as well as the Van Driest transformation in both the adiabatic and cooled situations. Table 5.3 omits values of S for data sets without points in the viscous sublayer. Values of C generally are close, but the robustness issues discussed in section 4 do reveal themselves in the data of Winter and Gaudet [1973] (`73020505`). Here, the first data is well above $Y^+ \approx 10$, and the proposed transformation's value of C is slightly above the Van Driest transformation's value of C. The proposed transformation works noticeably better than the Van Driest transformation in `72021501`. Here, the slope in the viscous sublayer is too low, and the proposed transformation corrects it within a reasonable experimental level of error.

5.3 Re_τ^* as a characteristic Reynolds number

As discussed in the introduction (chapter 1), the current paradigm supports Re_{δ_2} as a characteristic Reynolds number for these wall-bounded flows. But the proposed transformation

(a) `65050801`

(b) `72020205`

(c) `73020505`

Figure 5.4: Adiabatic experimental boundary layer cases, $B_q \approx 0$.

—————, incompressible boundary layer reference at $\mathrm{Re}_\tau = 1989$ from DNS by Sillero et al. [2013].

Circles, compressible boundary layer transformed by Van Driest transformation at Re_τ from stated experiment.

Diamonds, compressible boundary layer transformed by proposed transformation at Re_τ^* from stated experiment.
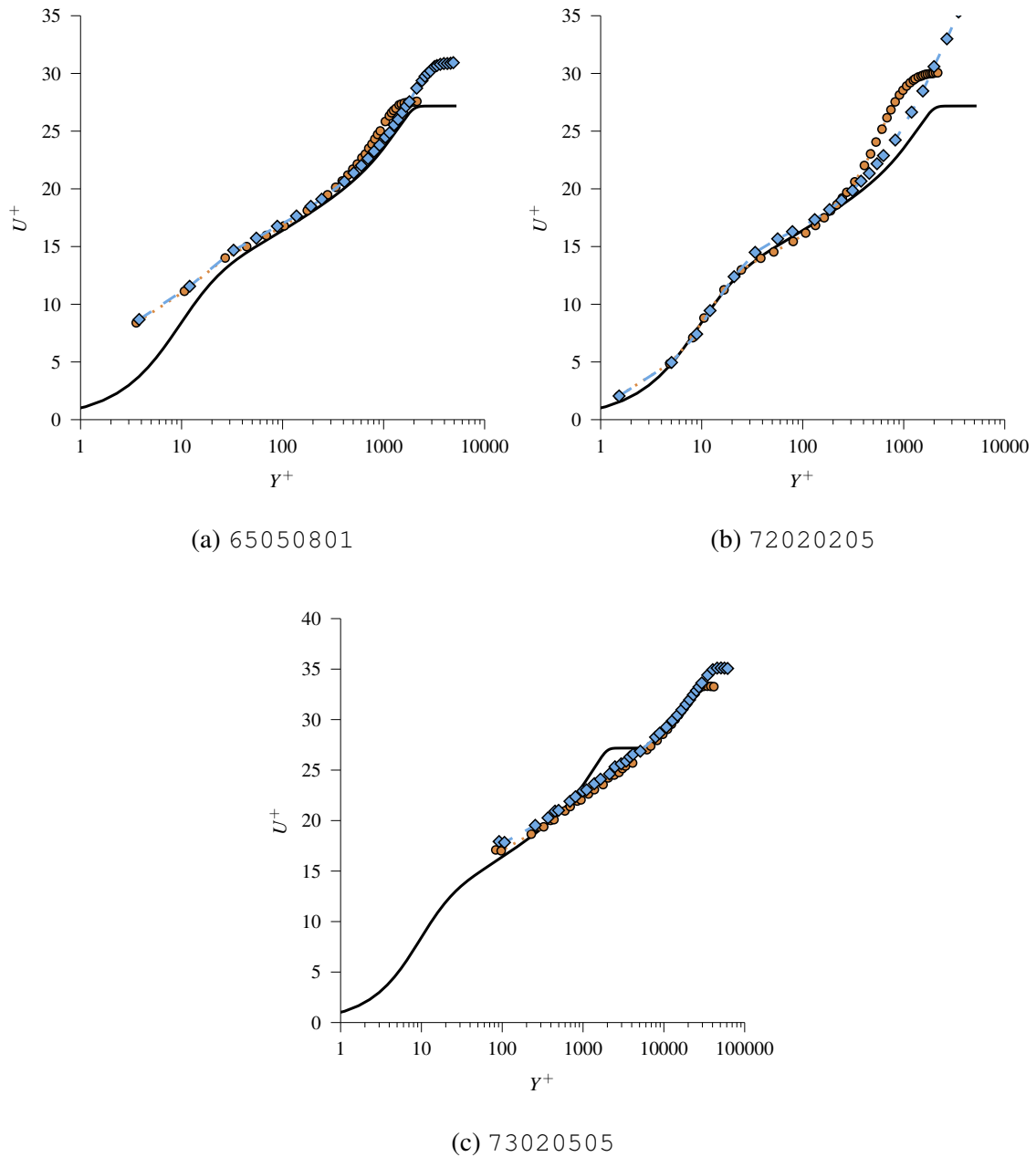
(a) `72021501`

(b) `7702S0301`
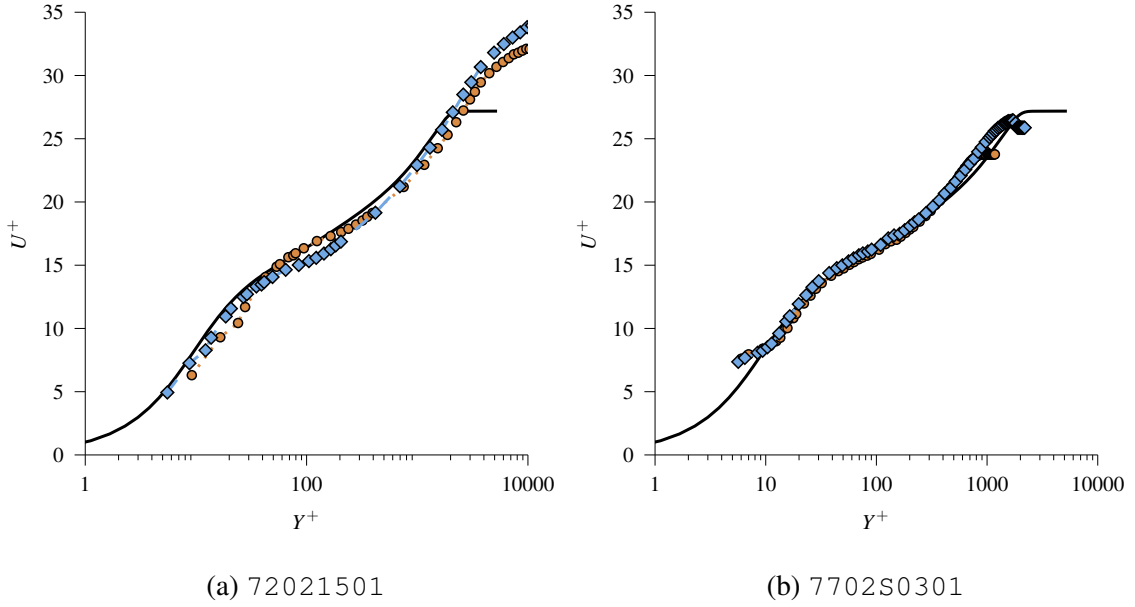
Figure 5.5: Cooled experimental boundary layer cases, $B_q < 0$.

- ———, incompressible boundary layer reference at $\text{Re}_\tau = 1989$ from DNS by Sillero et al. [2013].

- Circles, compressible boundary layer transformed by Van Driest transformation at Re_τ from stated experiment.

- Diamonds, compressible boundary layer transformed by proposed transformation at Re_τ^* from stated experiment.

also has a Reynolds number: its transformed friction Reynolds number Re_τ^*. The transformed friction Reynolds number for channels is

$$\text{Re}_\tau^* = \frac{\rho_c (\tau_w/\rho_c)^{1/2} h}{\mu_e} = \frac{h(\tau_w \rho_c)^{1/2}}{\mu_c} \tag{5.1}$$

and for boundary layers is

$$\text{Re}_\tau^* = \frac{\rho_e (\tau_w/\rho_e)^{1/2} \delta}{\mu_e} = \frac{\delta (\tau_w \rho_e)^{1/2}}{\mu_e} \tag{5.2}$$

which in both cases is the transformed coordinate Y^+ at the boundary layer thickness

Figure 5.6: Reynolds number effects in the log-law intercept
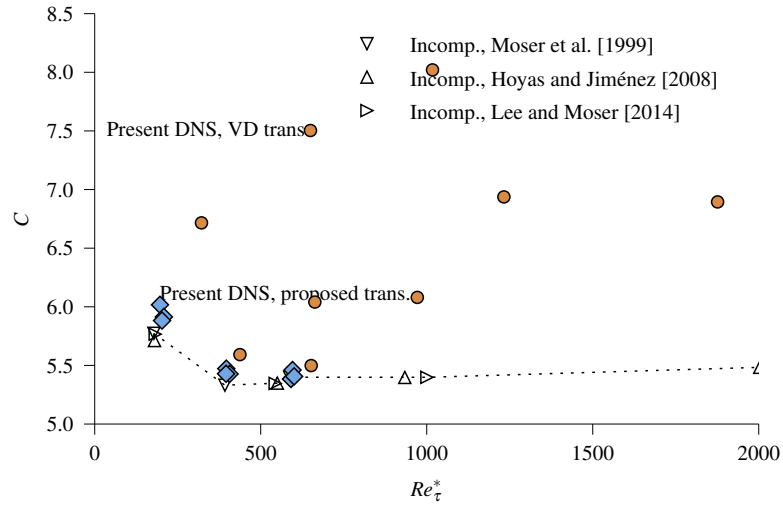

or the channel half-height.

This Reynolds number appears to properly characterize these wall-bounded flows. What does "properly characterize" mean? "Properly characterize" means that a compressible flow at Re_τ^* corresponds to the equivalent incompressible flow at Re_τ. A compressible flow's velocity profile transformed by the proposed transformation will match an equivalent incompressible flow with the same Re_τ^*.

This observation is more subtle that it appears. Consider the value of C. As already discussed in the numerical validation, the values of C from the proposed transformation match the incompressible case (they collapse the profile). But it is important to consider this collapse in a more global sense, to demonstrate the importance of Re_τ^* in characterizing a flow.

Figure 5.6 compares the performance of each transformation in matching the log-law intercept C (vertical axis) for a given transformed friction Reynolds number Re_τ^* (horizontal axis). This figure compares the transformed values of C to values of C from the incompressible channel flow DNS of Moser et al. [1999], Hoyas and Jiménez [2008], and Lee and Moser [2014]. The incompressible values of C increase for lower Reynolds numbers due to a low Reynolds number effect, and the transformed friction Reynolds number

Re_τ^* correctly picks up this low Reynolds number effect. This observation means that the proposed transformation accounts for Reynolds number effects as well, provided the transformed profile is compared to an equivalent incompressible profile with the same Re_τ^*.

The Van Driest transformed values of C (circles) blanket the figure, landing anywhere from 2 percent to 49 percent higher than the incompressible values at the same Re_τ. This disorder means that $\text{Re}_\tau = h\rho_w\sqrt{\tau_w/\rho_w}/\mu_w$ is a poor Reynolds number to describe the problem, unlike the proposed transformation's Re_τ^*. The proposed transformation's values of C (diamonds) cling to the incompressible trend line, varying only 4 percent higher than the incompressible reference at most, despite the large change in cooling rates. Compared to the closest incompressible DNS case in Moser et al. [1999], the $\text{Re}_\tau^* \approx 200$ cases are at most 4 percent off in C, the $\text{Re}_\tau^* \approx 400$ cases are at most 3 percent off in C, and the $\text{Re}_\tau^* \approx 600$ cases are at most 1 percent off in C, indicating that the proposed transformation more or less obtains the correct value of C.

The values of C_{VD} also appear to have a slight Reynolds number effect, but appear to level out when $\text{Re}_\tau > 400$. What this means is that the upwards shift in C_{VD} is not a Reynolds number effect, but is mostly due to wall cooling.

How do these results involving Re_τ^* fit into the current paradigm? Walz [1959] derived Re_{δ_2} by considering the skin friction and fluid inertia. Similarly, Re_τ^* does relate both inertia and wall friction. After some manipulation, it can be written as

$$\text{Re}_\tau^* = \left(\frac{c_f}{2}\right)^{1/2}\text{Re}_e \qquad (5.3)$$

so it is directly related to both the near-wall friction (through c_f) and the far-from-the-wall inertia (through Re_e).

5.4   Summary and future work

Early on in this thesis, the current paradigm of transformation concepts in compressible wall turbulence was discussed, and some of the ideas, while functional and adequate, seemed quite disconnected and piecemeal.

Now, with a new velocity transformation, and new characteristic Reynolds number, and a single coordinate (rather than two), the paradigm has united all the ideas underneath it. The derivations here connected many ideas that seemed entirely independent of each other. They connected (using mathematics) concepts like Morkovin's scaling, the "semi-local" scaling, the ideas behind the Van Driest transformation, and the ideas behind the viscous sublayer transformation under a single unified framework.

Still, many scientific questions remain unanswered. How well does this transformation perform in direct numerical simulations of boundary layers? In boundary layers, the heat transfer at the wall is completely disconnected from the Mach number, so it can be varied independently to quantify shifts in the velocity profile. How does this transformation perform at hypersonic Mach numbers? How does this transformation perform for incompressible flows with wall heating or wall cooling? How does this transformation perform for variable density flows with constant viscosity?

Engineering questions remain too, including how this new transformation could change existing skin friction formulas like Van Driest I (Van Driest [1951]) or Van Driest II (Van Driest [1955]).

These questions should drive future work. The only question left is how soon the answers will come.

Appendix A

Table of symbols

B_q Dimensionless wall heat transfer parameter (see equation 1.8).

C Log-law intercept. This thesis calculates it by a least squares fit using $\kappa = 0.41$ between $\mathrm{Re}_\tau^*/3$ and $\mathrm{Re}_\tau^*/4$.

c_f Skin friction. $c_f = \tau_w/(\frac{1}{2}\rho_e u_e^2)$.

c_p Specific heat at constant pressure.

ℓ_v Viscous length scale based on wall properties (see equation 3.2).

ℓ_x Streamwise channel length.

ℓ_y Wall normal channel length.

ℓ_z Lateral channel length.

h Channel half height. For Hybrid channels, $h = 1$.

k Thermal conductivity.

Ma Bulk Mach number for a channel. $\mathrm{Ma} = \langle u \rangle/(\gamma \bar{R} T_w)^{1/2}$.

Ma_c Centerline Mach number for a channel. $\mathrm{Ma}_c = u_c/(\gamma \bar{R} T_c)^{1/2}$.

Ma_e Edge Mach number for a boundary layer. $Ma_e = u_e/(\gamma \bar{R} T_e)^{1/2}$.

n Number of grid points.

Pr Prandtl number. $Pr = c_p \mu/k$.

q_w Heat flux through the wall.

r Dimensional, compressible and untransformed Reynolds stress.

R Dimensional, incompressible and transformed Reynolds stress.

r^+ Dimensionless, compressible and untransformed Reynolds stress. $r^+ = r/u_\tau^2$.

R^+ Dimensionless, incompressible and transformed Reynolds stress. $R^+ = R/u_\tau^2$.

$\bar{R}$ Specific gas constant.

Re_e Boundary layer edge Reynolds number. $Re_e = \rho_e u_e \delta/\mu_e$.

Re_h Bulk Reynolds number based on the channel half height. $Re_h = \langle \rho \rangle \langle u \rangle h/\mu_w$.

Re_{δ_2} $Re_{\delta_2} = \rho_e u_e \theta/\mu_w$.

Re_τ Friction Reynolds number based on wall properties. $Re_\tau = \rho_w u_\tau h/\mu_w$.

Re_τ^* Friction Reynolds number based on local properties and τ_w (see equation 5.1).

Re_θ $Re_\theta = \rho_e u_e \theta/\mu_e$.

S Average velocity gradient in the viscous sublayer up to $Y^+ = 4$.

T Temperature.

$\bar{T}$ Reynolds-averaged mean local temperature.

T_w Temperature at the wall. For Hybrid channels, $T_w = 1$.

T_c Reynolds-averaged channel centerline temperature.

T_e Reynolds-averaged boundary layer edge temperature.

u Dimensional, compressible and untransformed mean local velocity.

U Dimensional, incompressible and transformed mean local velocity.

u^+ Dimensionless, compressible and untransformed mean local velocity. $u^+ = u/u_\tau$.

U^+ Dimensionless, incompressible and transformed mean local velocity. $U^+ = U/u_\tau$. For the proposed velocity transformation, see equation 3.35.

u_c Reynolds-averaged channel centerline velocity.

$U^+_{\mathbf{VD}}$ Dimensionless Van Driest transformed velocity (see equation 1.6).

$U^+_{\mathbf{VS}}$ Dimensionless viscous sublayer transformed velocity (see equation 1.12).

u_τ Friction velocity based on wall properties (see equation 3.1).

u_e Reynolds-averaged mean boundary layer edge velocity.

$\langle u \rangle$ Mean velocity for entire channel. For Hybrid channels, $\langle u \rangle = 1$.

$\widetilde{u'_i u'_j}$ Favre-averaged Reynolds stress.

$\overline{\rho u''_i u''_j}$ Reynolds-averaged density-weighted Reynolds stress.

x Streamwise coordinate.

y Dimensional, compressible and untransformed wall normal coordinate.

Y Dimensional, incompressible and transformed wall normal coordinate.

y^+ Dimensionless, compressible and untransformed wall normal coordinate. $y^+ = y/\ell_v$.

Y^+ Dimensionless, incompressible and transformed wall normal coordinate. $Y^+ = Y/\ell_v$. For the proposed coordinate scaling, see equation 3.31.

y^* The "semi-local" scaling based on local properties and τ_w. For the proposed transfor-
    mation, $Y^+ = y^*$ (see equation 3.31).

z Lateral coordinate.

δ Boundary layer thickness.

δ_2 Momentum thickness.

γ Ratio of specific heats.

κ The von Kármán constant. For this thesis , $\kappa \approx 0.41$ for all calculations of C.

μ Viscosity.

$\bar{\mu}$ Reynolds-averaged mean local viscosity.

μ_w Viscosity at the wall. This value also serves as the incompressible value of viscosity.

ρ Density.

$\bar{\rho}$ Reynolds-averaged mean local density.

ρ_w Density at the wall. This value also serves at the incompressible value of density.

$\langle \rho \rangle$ Mean density for entire channel. For Hybrid channels, $\langle \rho \rangle = 1$.

τ Compressible shear stress.

τ^* Incompressible shear stress.

τ_w Shear stress at the wall.

θ Momentum thickness.

Appendix B

A short history of transformations in compressible wall turbulence

During the late 1940s to the early 1950s, several researchers initially developed several reasonably similar ideas that we now collectively call the Van Driest transformation. Van Driest [1951] provided a thorough analysis of skin friction in turbulent boundary layers, and during his analysis he noted the importance of density ratios in deriving a compressible equivalent to the logarithmic velocity distribution — a compressible form of the law of the wall, in other words. Wilson [1950], Young [1951], and Ferrari [1950] all have somewhat similar analyses with some parts of Van Driest's observations, but the accuracy of Van Driest's skin friction formula in Van Driest [1951] meant that this paper remains much more cited and consulted than these others, despite their similar content.

None of these early forms are the same as the integral Van Driest transformation we use today. That form came out slowly. Both Ferrari [1957] and Dorrance [1961] (also see Dorrance [1962]) contain obfuscated forms of the integral Van Driest transformation, but neither received much notice.

Other researchers picked up on Van Driest's compressible law of the wall and reformulated it as a transformation theory. The integral form of the Van Driest transformation

that we all use today (equation 1.6) was a generalization of Van Driest's law of the wall by Danberg [1964], who did the first large scale investigation of its performance. Many early papers assumed particular temperature-velocity relationships in their version of the Van Driest transformation. Danberg [1964] realized this limitation because he wanted to generalize the transformation to include porous surfaces, remarking in his section "Transformation of Compressible Velocity Profile (with Heat and Mass Transfer) into the Incompressible Velocity Profile" on page 61 that "Results of the compressible but zero mass transfer analysis of Van Driest [1951], Harkness [1959], and Moore [1962] can be produced from [equation 1.6]." Danberg realized that this equation was not a velocity profile or distribution but a method to transform compressible data into roughly equivalent incompressible data. Danberg's simplified form of the Van Driest transformation as given in figure 40 of Danberg [1964] is largely what is used today.

During this period in the 1960s and 1970s, before the Van Driest transformation became an accepted standard, Coles [1964] also represented an alternative, but it has not stood the test of time.

Danberg continued his analysis with the integral form of the Van Driest transformation in Danberg [1971] and one of his students used it in his dissertation (Sturek and Danberg [1971]). Other researchers, like Kemp and Owen [1972], began to compare the performance of this integral to the original Van Driest transformation and noticed similar results. Later review papers then began to call this integral form the Van Driest transformation and recommended its use (see Bushnell et al. [1977] and Fernholz et al. [1981]).

The viscous sublayer transformation's original derivation remains elusive, but several people have derived it over the years. Fernholz [1969] contains the same idea as it in a velocity distribution. The first reference to the viscous sublayer transformation in its modern integral form was in Carvin et al. [1988].

In the early 21st century, researchers began to see the limitations of the Van Driest transformation. Seeking to correct the Van Driest transformation, Brun et al. [2008] and

Transformation name	Velocity	Coordinate	Reynolds stress	Sources
Howarth		$\frac{dY}{dy} = \frac{\bar{\rho}}{\rho_w}$		Howarth [1948]
Cope and Hartree		$\frac{dY}{dy} = \frac{\mu_w}{\bar{\mu}}$		Cope and Hartree [1948]
Van Driest	$\frac{dU}{du} = \left(\frac{\bar{\rho}}{\rho_w}\right)^{1/2}$	$\frac{dY}{dy} = 1$		Van Driest [1951] and Danberg [1964]
Lobb et al.	$U^+ = \frac{u}{u_\tau^*}$	$Y^+ = \frac{y}{\ell_v^*}$		Lobb et al. [1955]
Morkovin			$R^+ = \frac{\bar{\rho}r}{\tau_w}$	Morkovin [1962]
Viscous sublayer	$\frac{dU}{du} = \frac{\bar{\mu}}{\mu_w}$	$\frac{dY}{dy} = 1$	$R^+ = 0$	Carvin et al. [1988]
Huang et al.		$Y^+ = \frac{y}{\ell_v^*}$		Huang et al. [1995]
Brun et al.	$\frac{dU}{du} = \frac{y}{Y}\left(\frac{\mu_w}{\bar{\mu}}\right)\left(\frac{\bar{\rho}}{\rho_w}\right)^{1/2}$	$\frac{dY}{dy} = \frac{\mu_w}{\bar{\mu}}$	$R = \left(\frac{y}{Y}\right)^2\left(\frac{\mu_w}{\bar{\mu}}\right)^2\left(\frac{\bar{\rho}}{\rho_w}\right)r$	Brun et al. [2008] and Haberkorn [2004]
"Howarth with log-law"	$\frac{dU}{du} = \frac{y}{Y}\left(\frac{\bar{\rho}}{\rho_w}\right)^{3/2}$	$\frac{dY}{dy} = \frac{\bar{\rho}}{\rho_w}$		Present thesis
Proposed	$\frac{dU}{du} = \left(\frac{\bar{\rho}}{\rho_w}\right)^{1/2}\left[1 + \frac{1}{2}\frac{1}{\bar{\rho}}\frac{d\bar{\rho}}{dy}y - \frac{1}{\bar{\mu}}\frac{d\bar{\mu}}{dy}y\right]$	$Y^+ = \frac{y}{\ell_v^*}$	$R_{uv}^+ = \frac{\bar{\rho}r_{uv}}{\tau_w}$	Present thesis

Table B.1: A history of transformations

Haberkorn [2004] sought to apply the transformation of Cope and Hartree [1948] to wall turbulence, arguing that it is related to the viscous sublayer transformation. This transformation, however, does not achieve a collapse to the incompressible law of the wall, but it was the first attempt to generalize a log-law condition to include any coordinate transformation.

Table B.1 lists many of the transformations considered over the years. Notice the transformation labeled "Howarth with log-law." This transformation uses the coordinate transformation of Howarth [1948] and is easy to think of in light of the transformation of Brun et al. [2008], and forms an equivalent transformation to this thesis's proposed one if mass conservation matters more than momentum conservation. But momentum transfer matters much more in wall turbulence, so this transformation works about as well as the transformation of Brun et al. [2008].

Bibliography

Iván Bermejo-Moreno, Julien Bodart, Johan Larsson, Blaise M. Barney, Joseph W. Nichols, and Steve Jones. Solving the compressible navier-stokes equations on up to 1.97 million cores and 4.1 trillion grid points. In *Proceedings of the International Conference on High Performance Computing, Networking, Storage and Analysis*, SC '13, pages 62:1–62:10, New York, NY, USA, 2013. ACM. ISBN 978-1-4503-2378-9. doi: 10.1145/2503210. 2503265.

Peter Bradshaw. Compressible turbulent shear layers. *Annual Review of Fluid Mechanics*, 9(1):33–52, 1977. ISSN 0066-4189. doi: 10.1146/annurev.fl.09.010177.000341.

Peter Bradshaw. Turbulence: the chief outstanding difficulty of our subject. *Experiments in Fluids*, 16(3-4):203–216, 1994. ISSN 0723-4864. doi: 10.1007/BF00206540.

Christophe Brun, Margareta Petrovan Boiarciuc, Marie Haberkorn, and Pierre Comte. Large eddy simulation of compressible channel flow. *Theoretical and Computational Fluid Dynamics*, 22(3-4):189–212, 2008. ISSN 0935-4964. doi: 10.1007/s00162-007-0073-y.

D.M. Bushnell, A.M. Cary, Jr., and J.E. Harris. Calculation methods for compressible turbulent boundary layers — 1976. Technical report, National Aeronautics and Space Administration, 1977. URL http://ntrs.nasa.gov/search.jsp?R=19780005428. NASA SP-422.

C. Carvin, J.F. Debieve, and A.J. Smits. The near-wall temperature profile of turbulent boundary layers. In *AIAA 26th Aerospace Sciences Meeting*, 1988. doi: 10.2514/6. 1988-136. AIAA-88-0136.

Tuncer Cebeci and A.M.O. Smith. *Analysis of Turbulent Boundary Layers*. Academic Press, 1974. ISBN 978-0124313040.

G. N. Coleman, J. Kim, and R. D. Moser. A numerical study of turbulent supersonic isothermal-wall channel flow. *Journal of Fluid Mechanics*, 305:159–183, 12 1995. ISSN 1469-7645. doi: 10.1017/S0022112095004587.

Donald Coles. The turbulent boundary layer in a compressible fluid. *Physics of Fluids*, 7 (9):1403–1423, 1964. ISSN 0031-9171. doi: 10.1063/1.1711395.

W. F. Cope and D. R. Hartree. The laminar boundary layer in compressible flow. *Philosophical Transactions of the Royal Society of London. Series A, Mathematical and Physical Sciences*, 241(827):1–69, 1948. ISSN 0080-4614.

James E. Danberg. *Characteristics of the turbulent boundary layer with heat and mass transfer at $M = 6.7$*. PhD thesis, Catholic University of America, 1964. Also AD0452471.

James E. Danberg. A re-evaluation of zero pressure gradient compressible turbulent boundary layer measurements. *AGARD Conference Proceedings*, 1971. ISSN 0549-7191. URL `http://www.dtic.mil/docs/citations/AD0737400`. Presented at Fluid Dynamics Panel Specialists' Meeting, London, September 13-15, 1971, No. 93 on Turbulent Shear Flows, AGARD-CP-93.

William H. Dorrance. Dissociation effects upon compressible turbulent boundary layer skin friction and heat transfer. *ARS Journal*, 31(1):61–70, January 1961. ISSN 1936-9972. doi: 10.2514/8.5385.

William H. Dorrance. *Viscous Hypersonic Flow: Theory of Reacting and Hypersonic Boundary Layers*. McGraw-Hill, 1962.

L. Duan, I. Beekman, and M.P. Martín. Direct numerical simulation of hypersonic turbulent boundary layers. part 2. effect of wall temperature. *Journal of Fluid Mechanics*, 655: 419–445, 7 2010. ISSN 1469-7645. doi: 10.1017/S0022112010000959.

L. Duan, I. Beekman, and M.P. Martín. Direct numerical simulation of hypersonic turbulent boundary layers. part 3. effect of mach number. *Journal of Fluid Mechanics*, 672:245–267, 4 2011. ISSN 1469-7645. doi: 10.1017/S0022112010005902.

H.H. Fernholz. Geschwindigkeitsprofile, temperaturprofile und halbempirische gesetze in kompressiblen turbulenten grenzschichten bei konstantem druck. *Ingenieur-Archiv*, 38 (4-5):311–328, 1969. ISSN 0020-1154. doi: 10.1007/BF00536174.

H.H. Fernholz and P.J. Finley. A critical compilation of compressible turbulent boundary layer data. Technical report, AGARD, 1977. URL `https://www.cso.nato.int/Pubs/rdp.asp?RDP=AGARD-AG-223`. AGARDograph no. 223, ADA045367.

H.H. Fernholz and P.J. Finley. A critical commentary on mean flow data for two-dimensional compressible turbulent boundary layers. Technical report, AGARD, 1980. URL `http://www.dtic.mil/docs/citations/ADA087704`. AGARDograph no. 253, ADA087704.

H.H. Fernholz, P.J. Finley, and V. Mikulla. A further compilation of compressible boundary layer data with a survey of turbulence data. Technical report, AGARD, 1981. URL `https://www.cso.nato.int/Pubs/rdp.asp?RDP=AGARD-AG-263`. AGARDograph no. 263, ADA111638.

Carlo Ferrari. Study of the boundary layer at supersonic speeds in turbulent flow: Case of flow along a flat plate. *Quarterly of Applied Mathematics*, 8, April 1950. ISSN 0033-569X.

Carlo Ferrari. Turbolenza di pabete. In Carlo Ferrari, editor, *Teoria della turbolenza*, volume 14 of *C.I.M.E. Summer Schools*, pages 171–286. Springer Berlin Heidelberg, 1957. ISBN 978-3-642-10908-9. doi: 10.1007/978-3-642-10910-2_7. Translation available as NASA republication RE 2-8-59W.

H. Foysi, S. Sarkar, and R. Friedrich. Compressibility effects and turbulence scalings in supersonic channel flow. *Journal of Fluid Mechanics*, 509:207–216, 6 2004. ISSN 1469-7645. doi: 10.1017/S0022112004009371.

Stephen E. Guarini, Robert D. Moser, Karim Shariff, and Alan Wray. Direct numerical simulation of a supersonic turbulent boundary layer at mach 2.5. *Journal of Fluid Mechanics*, 414:1–33, 7 2000. ISSN 1469-7645. doi: 10.1017/S0022112000008466.

Marie Haberkorn. *Simulation des grandes échelles en canal plan turbulent: effets de compressibilité et propagation acoustique*. PhD thesis, Université Louis Pasteur, 2004. URL http://perso.univ-lemans.fr/~yauregan/these/PhD_thesis_Haberkorn_2012.pdf.

John L. Harkness. Skin friction and heat transfer studies at supersonic speeds for turbulent boundary layers. Technical report, Defence Research Laboratory, the University of Texas at Austin, January 1959. DRL-435, CM-939.

L. Howarth. Concerning the effect of compressibility on laminar boundary layers and their separation. *Proceedings of the Royal Society of London. Series A. Mathematical and Physical Sciences*, 194(1036):16–42, 1948. doi: 10.1098/rspa.1948.0064.

Sergio Hoyas and Javier Jiménez. Reynolds number effects on the reynolds-stress budgets in turbulent channels. *Physics of Fluids (1994-present)*, 20(10), 2008. doi: http://dx.doi.org/10.1063/1.3005862.

P.G. Huang, G.N. Coleman, and P. Bradshaw. Compressible turbulent channel flows: Dns results and modelling. *Journal of Fluid Mechanics*, 305:185–218, 12 1995. ISSN 1469-7645. doi: 10.1017/S0022112095004599.

Mary W. Jackson, K.R. Czarnecki, and William J. Monta. Turbulent skin friction at high reynolds numbers and low supersonic velocities. Technical report, National Aeronautics and Space Administration, 1965. NASA technical note D-2687.

Javier Jiménez, Sergio Hoyas, Mark P. Simens, and Yoshinori Mizuno. Turbulent boundary layers and channels at moderate reynolds numbers. *Journal of Fluid Mechanics*, 657: 335–360, 8 2010. ISSN 1469-7645. doi: 10.1017/S0022112010001370.

Joseph H. Kemp, Jr. and F.K. Owen. Nozzle wall boundary layers at mach numbers 20 to 47. *AIAA Journal*, 10(7):872–879, 1972. ISSN 0001-1452. doi: 10.2514/3.50239.

Theodore von Kármán. Mechanische Ähnlichkeit und turbulenz. In *Nachrichten von der Gesellschaft der Wissenschaften zu Göttingen, Mathematisch-Physikalische Klasse*, pages 58–76, 1930. Translation available as NACA technical memo 611.

A.J. Laderman and A. Demetriades. Investigation of the structure of a cooled wall turbulent supersonic boundary layer. Technical report, Ford Aerospace and Communications Corporation, Aeronutronic Division, October 1977. URL `http://www.dtic.mil/docs/citations/ADA046365`. ADA046365.

M. Lagha, J. Kim, J. D. Eldredge, and X. Zhong. A numerical study of compressible turbulent boundary layers. *Physics of Fluids (1994-present)*, 23(1), 2011. doi: 10.1063/1.3541841.

Henry L. Langhaar. *Dimensional Analysis and Theory of Models*. Wiley, 1951. ISBN 978-0882756820.

Johan Larsson and Sanjiva K. Lele. Direct numerical simulation of canonical shock/turbulence interaction. *Physics of Fluids*, 21(12), 2009. doi: 10.1063/1.3275856.

Johan Larsson, Ivan Bermejo-Moreno, and Sanjiva K. Lele. Reynolds- and mach-number effects in canonical shock–turbulence interaction. *Journal of Fluid Mechanics*, 717: 293–321, 2 2013. ISSN 1469-7645. doi: 10.1017/jfm.2012.573.

Myoungkyu Lee and Robert D. Moser. Direct numerical simulation of turbulent channel flow up to $Re_\tau = 5200$. *Journal of Fluid Mechanics*, 2014. URL `http://arxiv.org/abs/1410.7809`. Under consideration for publication.

Sanjiva K. Lele. Compressibility effects on turbulence. *Annual Review of Fluid Mechanics*, 26(1):211–254, 1994. doi: 10.1146/annurev.fl.26.010194.001235.

R. Kenneth Lobb, Eva M. Winkler, and Jerome Persh. Nol hypersonic tunnel no. 4 results vii: experimental investigation of turbulent boundary layers in hypersonic flow. Technical report, U.S. Naval Ordnance Laboratory, White Oak, Maryland, March 1 1955. URL `http://www.dtic.mil/docs/citations/AD0068499`. NAVORD report 3880, AD0068499.

Thierry Maeder. *Numerical investigation of supersonic turbulent boundary layers*. PhD thesis, Swiss Federal Institute of Technology Zürich, 2000. URL `http://e-collection.library.ethz.ch/view/eth:23611`.

M. Pino Martín. Direct numerical simulation of hypersonic turbulent boundary layers. part 1. initialization and comparison with experiments. *Journal of Fluid Mechanics*, 570: 347–364, 1 2007. ISSN 1469-7645. doi: 10.1017/S0022112006003107.

A.S. Monin and A.M. Yaglom. *Statistical Fluid Mechanics: Mechanics of Turbulence*, volume 1. Dover, 1971. ISBN 987-0-486-45883-0.

Dave R. Moore. *Velocity similarity in the compressible turbulent boundary layer with heat transfer*. PhD thesis, University of Texas at Austin, June 1962.

Mark V. Morkovin. Effects of compressibility on turbulent flows. In *Mécanique de la turbulence*, pages 367–380. Paris, Éditions du Centre National de la Recherche Scientifique, 1962.

Robert D. Moser, John Kim, and Nagi N. Mansour. Direct numerical simulation of turbulent channel flow up to $re_\tau = 590$. *Physics of Fluids*, 11(4):943–945, 1999. ISSN 1070-6631. doi: 10.1063/1.869966.

Jie Pei, Jun Chen, Hussain Fazle, and ZhenSu She. New scaling for compressible wall turbulence. *Science China Physics, Mechanics and Astronomy*, 56(9):1770–1781, 2013. ISSN 1674-7348. doi: 10.1007/s11433-013-5147-9.

Sergio Pirozzoli and Matteo Bernardini. Probing high-reynolds-number effects in numerical boundary layers. *Physics of Fluids (1994-present)*, 25(2):021704, 2013. doi: 10.1063/1.4792164.

Sergio Pirozzoli, F. Grasso, and T.B. Gatski. Direct numerical simulation and analysis of a spatially evolving supersonic turbulent boundary layer at $m = 2.25$. *Physics of Fluids (1994-present)*, 16(3):530–545, 2004. ISSN 1070-6631. doi: 10.1063/1.1637604.

Ludwig Prandtl. Bericht über untersuchungen zur ausgebildeten turbulenz. *Zeitschrift für Angewandte Mathematik und Mechanik*, 5:136–139, April 1925. ISSN 1521-4001. URL http://ntrs.nasa.gov/archive/nasa/casi.ntrs.nasa.gov/20050029454.pdf. NACA technical memorandum 1231.

Ludwig Prandtl. Zur turbulenten strömung in rohren und längs platten. *Ergebnisse der Aerodynamischen Versuchsanstalt zu Göttingen*, 4:18–29, 1932. ISSN 1863-1088. URL http://webdoc.sub.gwdg.de/univerlag/2010/Prandtl_4.pdf.

Ludwig Prandtl. Neuere ergebnisse der turbulenzforschung. *Zeitschrift des Vereines Deutscher Ingenieure*, 7, 1933. ISSN 0341-7255. URL http://ntrs.nasa.gov/search.jsp?R=19930094697. NACA technical memorandum 720.

Juan A. Sillero, Javier Jiménez, and Robert D. Moser. One-point statistics for turbulent wall-bounded flows at reynolds numbers up to $\delta^+ \approx 2000$. *Physics of Fluids (1994-present)*, 25(10), 2013. doi: http://dx.doi.org/10.1063/1.4823831.

Alexander J. Smits and Jean-Paul Dussauge. *Turbulent Shear Layers in Supersonic Flow*. Springer, 2006. ISBN 978-3540288763.

E.F. Spina, Alexander J. Smits, and S.K. Robinson. The physics of supersonic turbulent boundary layers. *Annual Review of Fluid Mechanics*, 26:287–319, 1994. ISSN 0066-4189. doi: 10.1146/annurev.fl.26.010194.001443.

W.B. Sturek and J.E. Danberg. Experimental measurements of the supersonic turbulent boundary layerin a region of moderate adverse pressure gradient. In *AIAA 9th Aerospace Sciences Meeting*, January 25-27 1971. doi: 10.2514/6.1971-162. AIAA Paper No. 71-162.

Edward R. Van Driest. Turbulent boundary layer in compressible fluids. *Journal of the Aeronautical Sciences*, 18(3):1012–1028, 1951. ISSN 0022-4650. doi: 10.2514/2.7048.

Edward R. Van Driest. The turbulent boundary layer with variable prandtl number. In H. Görtler and W. Tollmien, editors, *50 Jahre Grenzschichtforschung*, pages 257–271. Braunschweig, 1955. 50 years of boundary layer research.

Robert L. Voisinet. Temperature-step effects on direct measurement of skin-friction drag. Technical report, Naval Surface Weapons Center, July 7 1977. URL `http://www.dtic.mil/docs/citations/ADA051340`. ADA051340.

Robert L. Voisinet and Roland E. Lee. Measurements of a mach 4.9 zero-pressure-gradient turbulent boundary layer with heat transfer. part 1. data compilation. Technical report, Naval Ordnance Lab, September 27 1972. URL `http://www.dtic.mil/docs/citations/AD0757330`. NOLTR 72-232 and AD0757330.

Alfred Walz. Näherungstheorie für kompressible turbulente grenzschichten. *ZAMM - Journal of Applied Mathematics and Mechanics / Zeitschrift für Angewandte Mathematik und Mechanik*, 36(S1):S50–S56, 1956. ISSN 1521-4001. doi: 10.1002/zamm.19560361317.

Alfred Walz. Compressible turbulent boundary layers with heat transfer and pressure gradient in flow direction. *Journal of Research of the National Bureau of Standards*, 63B: 53–72, 1959. doi: 10.6028/jres.063B.008. URL `http://nvlpubs.nist.gov/nistpubs/jres/63B/jresv63Bn1p53_A1b.pdf`.

Alfred Walz. Compressible turbulent boundary layers. In *Mécanique de la turbulence*, pages 299–352. Paris, Éditions du Centre National de la Recherche Scientifique, 1962.

Alfred Walz. *Boundary Layers of Flow and Temperature*. The M.I.T. Press, 1969.

Robert E. Wilson. Turbulent boundary-layer characteristics at supersonic speeds-theory and experiment. *Journal of the aeronautical sciences*, 17:585–594, 1950. ISSN 1936-9956. doi: 10.2514/8.1727.

Kenneth George Winter and L. Gaudet. Turbulent boundary-layer studies at high reynolds numbers at mach numbers between 0.2 and 2.8. Technical report, Aeronautical Research Council, 1973. A.R.C. reports and memoranda 3172.

A.D. Young. The equations of motion and energy and the velocity profile of a turbulent boundary layer in a compressible fluid. Technical report, The College of Aeronautic, Cranfield, January 1951. URL `https://dspace.lib.cranfield.ac.uk/handle/1826/7226`. Cranfield report no. 42.

You-Sheng Zhang, Wei-Tao Bi, Fazle Hussain, Xin-Liang Li, and Zhen-Su She. Mach-number-invariant mean-velocity profile of compressible turbulent boundary layers. *Phys. Rev. Lett.*, 109:054502, July 2012. doi: 10.1103/PhysRevLett.109.054502.